Applied Mathematics & Information Sciences
An International Journal

http://dx.doi.org/10.12785/amis/090201

Review of Polarization Observables in Incoherent Pion Photoproduction on the Deuteron

Eed M. Darwish[1,2,*]

[1] Physics Department, Faculty of Science, Sohag University, Sohag 82524, Egypt
[2] Physics Department, Faculty of Science, Taibah University, Al-Madinah Al-Munawarah, B.O. Box 30002, Saudi Arabia

Received: 2 May 2014, Revised: 3 Aug. 2014, Accepted: 5 Aug. 2014
Published online: 1 Mar. 2015

Abstract: Polarization observables in incoherent pion photoproduction from the deuteron are investigated in the energy region from π-threshold up to the $\Delta(1232)$-resonance with inclusion of all *leading* πNN effects. Formal expressions for polarization observables are derived and described by various beam, target and beam-target asymmetries for polarized photons and/or polarized deuterons. For the elementary pion photoproduction operator on the free nucleon, a realistic effective Lagrangian approach is used which includes seven nucleon resonances, in addition to Born and vector-meson exchange terms. The interactions in the final two-body subsystems are taken from separable representations of realistic potentials. Results are given for the unpolarized cross sections, the doubly polarized cross sections for parallel and antiparallel helicity states, the linear photon asymmetry, the double polarization E-asymmetry and, the vector and tensor deuteron asymmetries for the $\gamma\mathbf{d} \to \pi^- pp$, $\gamma\mathbf{d} \to \pi^+ nn$, and $\gamma\mathbf{d} \to \pi^0 np$ channels. The contributions to the spin asymmetry and the Gerasimov-Drell-Hearn (GDH) integral from separate channels are evaluated by explicit integration up to a photon lab-energy of 350 MeV. Effects of final-state interaction are investigated and their role in these observables are found to be significant, specially for π^0 production. The extracted results are compared with available experimental data and predictions of other works, and a satisfactory agreement is obtained. The sensitivity of the $\gamma d \to \pi NN$ results to the elementary $\gamma N \to \pi N$ operator is also investigated and a considerable dependence is found. This indicates that it can serve as a filter for different elementary operators. We expect that the results presented here may be useful to interpret the recent measurements from the high-intensity and high duty-factor electron accelerators MAMI, ELSA, Jefferson Lab, LEGS, and MAX-Lab.

Keywords: Meson production, Photoproduction reactions, Few-Body Systems, Polarized beams, Polarized targets, Spin observables, Sum rules, Final-state interactions

1 Introduction

The study of pseudoscalar meson production in electromagnetic reactions on light nuclei has become a very active field of research in medium-energy nuclear physics with respect to the study of hadron structure. For the following reasons the deuteron plays an outstanding role besides the free nucleon. The first one is that the deuteron is the simplest nucleus on whose structure we have abundant information and a reliable theoretical understanding, i.e., the structure of the deuteron is very well understood in comparison to heavier nuclei. Furthermore, the small binding energy of nucleons in the deuteron, which from the kinematical point of view provides the case of a nearly free neutron target, allows one to compare the contributions of its constituents to the electromagnetic and hadronic reactions to those from free nucleons in order to estimate interaction effects.

Meson photo- and electroproduction on light nuclei is primarily motivated by the following possibilities: (i) study of the elementary neutron amplitude in the absence of a free neutron target, (ii) investigation of medium effects, i.e., possible changes of the production operator in the presence of other nucleons, (iii) it provides an interesting means to study nuclear structure, and (iv) it gives information on pion production on off-shell nucleon, as well as on the very important ΔN-interaction in a nuclear medium.

The major reason for studying polarization phenomena lies in the fact that only the use of polarization degrees of freedom allows one to obtain complete information on all possible reaction matrix

* Corresponding author e-mail: eeddarwish@yahoo.com

elements. Without polarization, the cross section is given by the incoherent sum of squares of the reaction matrix elements only. Thus, small amplitudes are masked by the dominant ones. On the other hand, small amplitudes very often contain interesting information on subtle dynamical effects. This is the place where polarization observables enter, because such observables in general contain interference terms of the various matrix elements in different ways. Thus, a small amplitude may be considerably amplified by the interference with a dominant matrix element.

The earliest calculations for pion photoproduction from the deuteron were performed using the impulse approximation (IA) [1,2]. Approximate treatments of final-state interaction (FSI) effects within a diagrammatic approach have been reported in Refs. [3,4,5]. Photoproduction of pions from the deuteron has been investigated with the spectator nucleon model [6] ignoring all kinds of FSI and two-body processes. The NN-FSI is considered in Ref. [7] and a good agreement with experiment was obtained. The influence of NN- and πN-rescattering on the unpolarized cross sections is investigated in Refs. [8,9], whereas the role of the $N\Delta$-FSI in pion photoproduction from the deuteron is investigated in [10]. It has been shown that full calculations with the off-shell amplitudes of NN- and $N\Delta$-FSI are necessary to obtain a quantitative description of the cross sections.

Most of calculations have treated only unpolarized observables, like the differential and total cross sections. These cross sections provide information only regarding the sum of the absolute squares of the amplitudes, whereas the polarization observables allow extraction of more information. Observables with a polarized photon beam and/or polarized deuteron target have not been throughly investigated. Recent years have witnessed an increasing interest in theoretical research on meson electromagnetic production including polarization observables. This interest is partly due to the new generation of high-intensity and high duty-cycle electron accelerators, such as MAMI at Mainz and ELSA at Bonn (Germany), JLab at Newport News (USA), and MAX-Lab at Lund (Sweden) as well as laser backscattering facilities such as GRAAL at Grenoble (France) and LEGS at Brookhaven (USA) - for an experimental overview see Refs. [11,12,13,14]. With the development of these new facilities, it is now possible to obtain accurate data for meson electromagnetic production, including single and double spin-dependent observables.

Polarization observables for π^--photoproduction on the deuteron via the reaction $d(\gamma,\pi^-)pp$ have been studied within a diagrammatic approach [15]. In [8,9], the energy dependence of the three charge states of the pion for incoherent pion photoproduction on the deuteron in the $\Delta(1232)$-resonance region has been investigated. Results for differential and total cross sections and the beam-target spin asymmetry which determines the Gerasimov-Drell-Hearn (GDH) sum rule were given. In Refs. [16,17,18], we have investigated various single- and double-polarization asymmetries in incoherent pion photoproduction from the deuteron without any kind of FSI effects. We found that interference of Born terms and the $\Delta(1232)$-contribution plays a significant role in the calculations. The vector target asymmetry T_{11} has been found to be very sensitive to this interference. Furthermore, our results for the linear photon asymmetry [18] have been compared with the preliminary experimental data from the LEGS Spin Collaboration [14] and major discrepancies were evident. Since a strong influence of the FSI on the unpolarized cross sections was found in [8,9], one might expect that the LEGS data can be understood in terms of the FSI and possibly two-body effects.

Therefore, we have investigated the influence of NN-FSI on the helicity structure (Ref. [19]) and the linear photon asymmetry (Ref. [20]) of the $\gamma\mathbf{d} \to \pi^- pp$ reaction. The differential polarized cross-section difference for the parallel and antiparallel helicity states has been predicted and compared with recent experimental data from MAMI (Mainz/Pavia) [12]. It has been shown that the effect of NN-rescattering is much less important in the polarized differential cross-section difference than in the unpolarized one. It has been also found in [20], that NN-FSI is quite important and leads to a better agreement with existing experimental data. In addition, we have investigated in Ref. [21] the role of the NN-rescattering effect on several single- and double-polarization observables of photon and deuteron target in π^--photoproduction from the deuteron with polarized photon beam and/or oriented deuteron target. The understanding of this mechanism is of great importance to understand the basic NN interaction. Based on the effective Lagrangian model [6], the helicity dependence of the $\gamma\mathbf{N} \to \pi N$ reaction channels is investigated in Ref. [22] and compared with recent experimental data from the GDH Collaboration, and a good agreement was obtained. The work in [9] was improved by Arenhövel *et al.* [23,24] and by Levchuk *et al.* [25], where a better elementary production operators provided by MAID [26] and SAID [27], respectively, were employed and FSI effects were considered. Explicit evaluation of the deuteron spin asymmetry and the associated GDH sum rule were presented in said work.

The A2 and GDH Collaborations at MAMI have undertaken a joint effort to verify experimentally the GDH sum rule [28], measuring the difference between the helicity components in both the total $[\sigma^P - \sigma^A]$ and the differential $[d(\sigma^P - \sigma^A)/d\Omega]$ photoabsorption cross sections, where $\sigma^{P,A}$ stands for the parallel and antiparallel spin orientations of the photon and target deuteron. In these experiments, circularly polarized photons are scattered on longitudinally polarized deuterons to determine the double polarization asymmetry in a large kinematical range [12]. These helicity dependent cross sections provide valuable

information on the nucleon spin structure and allow to extract information on the neutron. The knowledge of these cross sections is also required to test the validity of the GDH sum rule on the deuteron and the neutron as well as to explore which are the dominant contributions to the GDH integral. These new measurements will make possible to test experimentally the behavior of the GDH integral.

However, in order to explore the contributions of the resonances, the total photoabsorption cross section does not provide enough information. Fixing degrees of freedom by selection of particular partial reaction channels allows to obtain more detailed information. This is possible with double polarization observables of the differential cross section. The present focus of the LEGS Collaboration is the measurement of double polarization spin observables in photoreactions on the proton, the neutron, and the deuteron. For instance, the beam-target double polarization E-asymmetry of the $\gamma\mathbf{d} \to \pi^0 np$ reaction at photon lab-energy $E_\gamma = 349 \pm 5$ MeV, has been recently measured [14]. This asymmetry will certainly provide an important test, which, indirectly, allows to check our knowledge on the process of pion production from the neutron. To the best of our knowledge, there is no calculation in the literature for the double polarization E-asymmetry of the $\gamma\mathbf{d} \to \pi NN$ reaction channels.

Theoretical predictions for the unpolarized cross sections and polarization observables of the processes $\gamma\mathbf{d} \to \pi^- pp$, $\gamma\mathbf{d} \to \pi^+ nn$, and $\gamma\mathbf{d} \to \pi^0 np$, in the energy range from π-threshold up to the $\Delta(1232)$-resonance, were performed in Refs. [19,20,21] and extended in Refs. [29,30] using as elementary $\gamma N \to \pi N$ reaction a realistic effective Lagrangian approach (ELA) from [31]. This elementary reaction model provides a reliable description of the π-threshold region. Numerical results for unpolarized cross sections and various polarization observables have been presented [29,30] where in addition to the pure IA and NN-FSI, the πN-rescattering is also included. Extension of our previous works [17,18, 19,20,21,22] to the π-threshold region was given in order to understand the dynamics of the pion photoproduction amplitude near π-threshold. It was found in [29,30] that the results for unpolarized cross sections and spin asymmetries are strongly dependent on the elementary $\gamma N \to \pi N$ operator.

The calculations presented in this review are of high interest in view of the extensive recent polarization measurements from A2 and GDH@MAMI [12] and LEGS@BNL [14] Collaborations. A theoretical understanding of these data on the deuteron target will provide information about the pion photoproduction from the neutron reaction, which is not well known yet, but is required for a complete understanding of Δ-excitations in the pion photoproduction process.

This review is structured as follows: in the next section we briefly outline the electromagnetic and hadronic two-body elementary reactions which we include in our treatment of pion photoproduction from the deuteron. In section 3, a brief review of the framework for the reaction $d(\gamma,\pi)NN$ in which the transition matrix elements are calculated [8] is presented. The main results for the $\gamma\mathbf{d} \to \pi^- pp$, $\gamma\mathbf{d} \to \pi^+ nn$, and $\gamma\mathbf{d} \to \pi^0 np$ reactions together with a comparison to experimental data and other theoretical predictions are presented in section 4. In addition, the sensitivity of our results to the elementary pion photoproduction operator is discussed here. Finally, we close with some conclusions and an outlook in section 5. Throughout this work we use natural units $\hbar = c = 1$.

2 Elementary electromagnetic and hadronic reactions

In this section, we will briefly describe the necessary ingredients for the various elementary reactions which govern the process of incoherent pion photoproduction from the deuteron. These are the pion photoproduction from free nucleons $\gamma N \to \pi N$, which plays the central part in the reaction, and hadronic two-body scattering reactions, namely nucleon-nucleon ($NN \to NN$) and pion-nucleon ($\pi N \to \pi N$) scattering, which constitute the rescattering effects in the final state.

The elementary reactions are classified as two-body reactions. The general form of these reactions is given by

$$a(p_a) + b(p_b) \to c(p_c) + d(p_d)\,, \tag{1}$$

where $p_i = (E_i, \mathbf{p}_i)$ denotes the four-momentum of particle "i" with $i \in \{a,b,c,d\}$. Particles a and b stand for a photon and a nucleon in the case of pion photoproduction from free nucleons, a pair of baryons in the case of NN scattering, or a meson and a baryon in the case of πN scattering. Corresponding assignments stand for the final particles c and d.

Following the conventions of Bjorken and Drell [32] the general form for the differential cross section of a two-particle reaction in the center of mass (c.m.) system is given by

$$\frac{d\sigma}{d\Omega_c} = \frac{1}{4\pi^2 W^2} \frac{E_a E_b E_c E_d}{\tilde{F}_a \tilde{F}_b \tilde{F}_c \tilde{F}_d} \frac{p_c}{p_a} \frac{1}{s} \times \sum_{\mu_d \mu_c \mu_b \mu_a} \left| \mathscr{M}^{fi}_{\mu_d \mu_c \mu_b \mu_a}(\mathbf{p}_d, \mathbf{p}_c, \mathbf{p}_b, \mathbf{p}_a) \right|^2$$

with $\mathscr{M}^{fi}_{\mu_d \mu_c \mu_b \mu_a}$ the reaction matrix, μ_i denotes the spin projection of particle "i", and $\tilde{F}_i$ is a factor arising from the covariant normalization of the states and its form depends on whether the particle is a boson ($\tilde{F}_i = 2E_i$) or a fermion ($\tilde{F}_i = E_i/m_i$), where E_i and m_i are its energy and mass, respectively. The factor $s = (2s_a + 1)(2s_b + 1)$ takes into account the averaging over the initial spin states, where s_a and s_b denote the spins of the incoming particles a and b, respectively. If particle a is a real photon, then $s_A = 1/2$

because the real photon is a boson with two polarization states. All momenta are functions of the invariant mass of the two-body system W, i.e. $p_i = p_i(W)$.

For the scattering processes, it is more convenient to use non-covariant normalization of the states and to switch to a coupled spin representation replacing the $\mathscr{M}$-matrix by the $\mathscr{T}$-matrix via

$$\mathscr{M}^{fi}_{\mu_d\mu_c\mu_b\mu_a}(\mathbf{p}_d,\mathbf{p}_c,\mathbf{p}_b,\mathbf{p}_a) = (2\pi)^3\sqrt{\tilde{F}_a\tilde{F}_b\tilde{F}_c\tilde{F}_d} \times \sum_{S'\mu'_{S'}S\mu_S} C^{s_cs_dS'}_{\mu_c\mu_d\mu'_{S'}} C^{s_as_bS}_{\mu_a\mu_b\mu_S}\mathscr{T}^{fi}_{S'\mu'_{S'}S\mu_S}(\mathbf{p}_d,\mathbf{p}_c,\mathbf{p}_b,\mathbf{p}_a), \quad (2)$$

with $C^{s_cs_dS'}_{\mu_c\mu_d\mu'_{S'}}$ the appropriate Clebsch-Gordan coefficient. The partial wave representation of the $\mathscr{T}$-matrix reads

$$\mathscr{T}^{fi}_{S'\mu'_{S'}S\mu_S}(W,\mathbf{p}',\mathbf{p}) = \sum_{\ell'\ell J} X^{\ell'\ell J}_{S'\mu'_{S'}S\mu_S}(\hat{p}',\hat{p})\, T^{fi}_{\ell'\ell J}(W,p',p), \quad (3)$$

where we have introduced

$$X^{\ell'\ell J}_{S'\mu'_{S'}S\mu_S}(\hat{p}',\hat{p}) = \sum_{\mu'_{\ell'}\mu_\ell\mu_J} C^{\ell'S'J}_{\mu'_{\ell'}\mu'_{S'}\mu_J} C^{\ell SJ}_{\mu_\ell\mu_S\mu_J} \times Y_{\ell'\mu'_{\ell'}}(\hat{p}')\, Y^*_{\ell\mu_\ell}(\hat{p}). \quad (4)$$

Here ℓ and J denote, respectively, the orbital and total angular momenta of the system. $Y_{\ell\mu}(\hat{p})$ is the spherical harmonic, $\mathbf{p}'$ and $\mathbf{p}$ are the final and initial relative momenta, respectively, and $\hat{p} = (\theta_\mathbf{p}, \phi_\mathbf{p})$.

The partial wave T-matrix is obtained as a solution of the Lippmann-Schwinger (LS) equation [33]

$$T^{fi}_{\ell'\ell J}(W,p',p) = V^{fi}_{\ell'\ell J}(p',p) + \sum_{n\ell''} 2m_n \int_0^\infty dp''_n\, (p''_n)^2 \frac{V^{fn}_{\ell'\ell''J}(p',p''_n)\, T^{ni}_{\ell''\ell J}(W,p''_n,p)}{q_n^2 - (p''_n)^2 + i\varepsilon}, \quad (5)$$

where $V^{fi}_{\ell'\ell J}(p',p)$ is the interaction potential between the particles and "n" labels possible intermediate two-particle configurations with total mass M_n, reduced mass m_n, and with relative momentum $q_n = \sqrt{2m_n(W-M_n)}$ in the c.m. system. Now we will briefly review the different elementary processes in some detail.

2.1 Pion photoproduction from free nucleons

To study the $\gamma d \to \pi NN$ processes we first need a model for the elementary reaction $\gamma N \to \pi N$. The model we use for this elementary process is the one elaborated in Ref. [31], which has been applied successfully from π-threshold up to 1 GeV of photon energy in the laboratory reference system.

The model is based upon an effective Lagrangian approach (ELA) which from a theoretical point of view is a very appealing, reliable, and formally well-established approach in the energy region of the mass of the nucleon. It includes Born terms (diagrams (A)-(D) in Fig. (1)), vector-meson exchanges (ρ and ω, diagram (E) in Fig. (1)), and all the four star resonances in Particle Data Group (PDG) [34] up to 1.7 GeV and up to spin-3/2: $\Delta(1232)$, N(1440), N(1520), N(1535), $\Delta(1620)$, N(1650), and $\Delta(1700)$ (diagrams (F) and (G) in Fig. (1)).

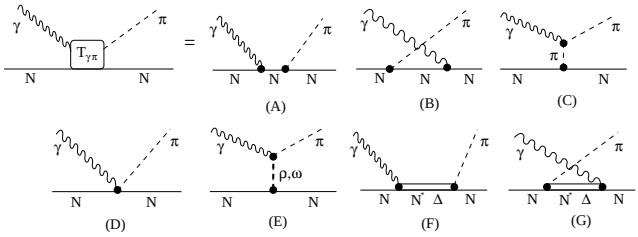

Fig. 1: Feynman diagrams for pion photoproduction from free nucleons. Born terms: (A) direct nucleon pole or s-channel, (B) crossed nucleon pole or u-channel, (C) pion in flight or t-channel, and (D) Kroll-Rudermann contact term; (E) vector meson exchange; resonance excitations: (F) direct or s-channel and (G) crossed or u-channel.

In the pion photoproduction model from free nucleons [31] it was assumed that final-state interaction (FSI) factorize and can be included through the distortion of the πN final-state wave function (pion-nucleon rescattering). πN-FSI was included by adding a phase δ_{FSI} to the electromagnetic multipoles. This phase is set so that the total phase of the multipole matches the total phase of the energy dependent solution of SAID [27]. In this way it was possible to isolate the contribution of the bare diagrams to the physical observables. The parameters of the resonances were extracted from data fitting the electromagnetic multipoles from the energy independent solution of SAID [27] applying a modern optimization technique based upon genetic algorithms combined with gradient based routines [31,35] which provides reliable values for the parameters of the nucleon resonances. Once the bare properties of the nucleon resonances have been extracted from data, their contribution to more complex problems can be calculated.

2.2 Nucleon-nucleon scattering

For a given NN potential V, the T-matrix of the NN-scattering is obtained from the LS equation which in partial wave decomposition reads

$$T_\ell(p',p;E) = V_\ell(p',p) + \int_0^\infty dk k^2\, V_\ell(p',k) \frac{M_N}{M_N E - k^2 + i\varepsilon} T_\ell(k,p;E) \quad (6)$$

for single channels. For the coupled channels it reads

$$T_{\ell\ell'}(p',p;E) = V_{\ell\ell'}(p',p) + \sum_{\ell''}\int_0^\infty dk k^2\, V_{\ell\ell''}(p',k)\frac{M_N}{M_N E - k^2 + i\varepsilon} T_{\ell''\ell'}(k,p;E)\,, \tag{7}$$

where **p**, **k** and **p**′ are the relative three-momenta of the two interacting nucleons in the initial, intermediate and final state, respectively. E denotes the energy of the two interacting nucleons in the c. m. frame and is given by $E = p_0^2/M_N$, where p_0 is the c. m. on-shell momentum.

Using the identity

$$\frac{1}{x - x_0 + i\varepsilon} = \mathscr{P}\frac{1}{x - x_0} - i\pi\delta(x - x_0)\,, \tag{8}$$

where $\mathscr{P}$ denotes the principal value integral, we get the T-matrix elements in partial wave decomposition

$$\begin{aligned} T_\ell(p',p;E) &= V_\ell(p',p) \\ &+ \mathscr{P}\int_0^\infty dk k^2\, V_\ell(p',k)\frac{M_N}{p_0^2 - k^2} T_\ell(k,p;E) \\ &- \frac{1}{2} i\pi M_N p_0 V_\ell(p',p_0) T_\ell(p_0,p;E) \end{aligned} \tag{9}$$

for single channels and

$$\begin{aligned} T_{\ell\ell'}(p',p;E) &= V_{\ell\ell'}(p',p) \\ &+ \sum_{\ell''=J\pm1} \mathscr{P}\int_0^\infty dk k^2\, V_{\ell\ell''}(p',k)\frac{M_N}{p_0^2 - k^2} T_{\ell''\ell'}(k,p;E) \\ &- \frac{1}{2} i\pi M_N p_0 V_{\ell\ell'}(p',p_0) T_{\ell\ell'}(p_0,p;E) \end{aligned} \tag{10}$$

for coupled channels. These one-dimensional integral equations can be solved numerically by means of a matrix inversion algorithm which is explained in Ref. [36].

For the NN interaction in the NN-subsystem, the separable representations of the realistic Paris potential from [37] are used in this work. These separable interactions represent a good approximation of the on-shell as well as off-shell properties of the original Paris potential and show a good fit to the modern NN data base. Thus, the use of such a realistic potential is good enough for our purpose.

2.3 Pion-nucleon scattering

Analogous to the case of NN-scattering, the T-matrix for πN scattering is obtained from the LS equation

$$\begin{aligned} T(p',p;E) &= V(p',p) \\ &+ \int_0^\infty dk k^2\, V(p',k)\, \mathscr{G}_{\pi N}(k,E)\, T(k,p;E)\,, \end{aligned} \tag{11}$$

with the πN propagator

$$\mathscr{G}_{\pi N}(k,E) = \frac{1}{E - E_\pi(k) - E_N(k) + i\varepsilon}\,, \tag{12}$$

where **p**, **k** and **p**′ are the πN relative momentum in the initial, intermediate and final state, respectively; and $p \equiv |\mathbf{p}|$, $k \equiv |\mathbf{k}|$ and $p' \equiv |\mathbf{p}'|$. $E = \sqrt{M_N^2 + p_0^2} + \sqrt{m_\pi^2 + p_0^2}$ denotes the total collision energy with on-shell momentum p_0 in the c.m. frame. For our calculations, relativistic kinematics for both pion and nucleon are used, thus

$$E_\pi(k) = \sqrt{m_\pi^2 + k^2}\,, \qquad E_N(k) = \sqrt{M_N^2 + k^2}\,. \tag{13}$$

The partial wave T-matrix for πN scattering is then given by

$$\begin{aligned} T(p',p;E) &= V(p',p) \\ &+ \int_0^\infty dk k^2\, V(p',k)\frac{G(k)}{p_0^2 - k^2 + i\varepsilon} T(k,p;E)\,, \end{aligned} \tag{14}$$

where

$$G(k) = \frac{[E_N(p_0) + E_N(k)]\,[E_\pi(p_0) + E_\pi(k)]}{[E_N(p_0) + E_N(k) + E_\pi(p_0) + E_\pi(k)]}\,. \tag{15}$$

To transform this equation into a principal value integral equation using identity (8) to get the matrix elements in partial wave decomposition as

$$\begin{aligned} T(p',p;E) &= V(p',p) \\ &+ \mathscr{P}\int_0^\infty dk k^2\, V(p',k)\frac{G(k)}{p_0^2 - k^2} T(k,p;E) \\ &- \frac{1}{2} i\pi p_0 G(p_0) V(p',p_0) T(p_0,p;E)\,. \end{aligned} \tag{16}$$

This one-dimensional integral equation can be solved numerically for a given πN potential model $V(p',p)$ by using the matrix inversion method [36].

For the πN potential, the realistic separable representation of πN interaction of Nozawa *et al.* [38] is used. This model is consistent with the existing unitary description of the πNN system and treats the πN interaction dynamically, with all S-, P- and D-wave πN phase shifts being well reproduced below 500 MeV.

3 Theoretical treatment of the $\gamma d \to \pi NN$ reaction

3.1 Kinematics and cross section

As a starting point, we will first consider the formalism for incoherent single pion photoproduction from the deuteron

$$\gamma(k,\varepsilon_\mu) + d(d) \to \pi(q) + N_1(p_1) + N_2(p_2)\,, \tag{17}$$

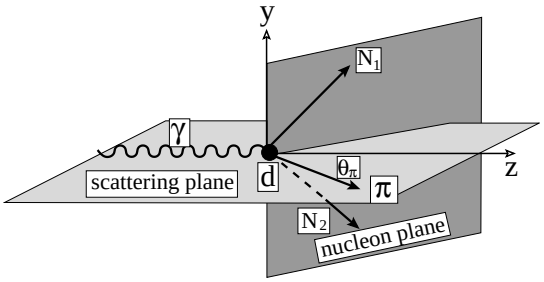

Fig. 2: The kinematics of incoherent pion photoproduction from the deuteron in the laboratory frame.

where the four-momenta of the participating particles are indicated in the parentheses. The polarization vector of the photon is denoted by ε_μ ($\mu = \pm 1$).

The general expression of the fivefold differential cross section is given by [32]

$$d^5\sigma = \frac{\delta^4(k+d-q-p_1-p_2)\,M_N^2\,d^3q d^3p_1 d^3p_2}{96\,(2\pi)^5\,|\mathbf{v}_\gamma - \mathbf{v}_d|\,E_\gamma E_d E_1 E_2\,\omega_q} \times \sum_{sm\mu m_d} \left|T_{sm\mu m_d}(\mathbf{q},\mathbf{p}_1,\mathbf{p}_2,\mathbf{d},\mathbf{k})\right|^2 , \tag{18}$$

where the definition of all kinematical variables and quantum numbers is given in Ref. [8]. For the calculation of the cross sections, the deuteron rest frame is utilized. We have chosen a right-handed coordinate system where the z-axis is defined by the photon momentum $\mathbf{k}$ and the y-axis by $\mathbf{k}\times\mathbf{q}$, where $\mathbf{q}$ is the pion momentum. The kinematical situation is shown in Fig. (2). The scattering plane is defined by the momenta of photon $\mathbf{k}$ and pion $\mathbf{q}$ whereas the momenta of the two outgoing nucleons $\mathbf{p}_1$ and $\mathbf{p}_2$ define the nucleon plane. As independent variables for the characterization of the final state, the outgoing pion momentum $\mathbf{q} = (q,\theta_\pi,\phi_\pi)$ is chosen. Furthermore, the spherical angles $\Omega_p = (\theta_p,\phi_p)$ of the relative momentum $\mathbf{p} = (\mathbf{p}_1 - \mathbf{p}_2)/2 = (p,\Omega_p)$ of the two outgoing nucleons.

The semi-inclusive differential cross section, where only the final pion is detected without analyzing its energy, is obtained from (18)

$$\frac{d^2\sigma}{d\Omega_\pi} = \int_0^{q_{max}} dq \int d\Omega_p \,\frac{\rho_s}{6} \sum_{sm\mu m_d} \left|T_{sm\mu m_d}(\mathbf{q},\mathbf{p},\mathbf{k})\right|^2 , \tag{19}$$

where the maximum pion momentum q_{max} is determined by the kinematics and ρ_s is a phase space factor.

3.2 The photoproduction amplitude

All observables are determined by the photoproduction amplitude $T_{sm\mu m_d}$ of the electromagnetic pion production

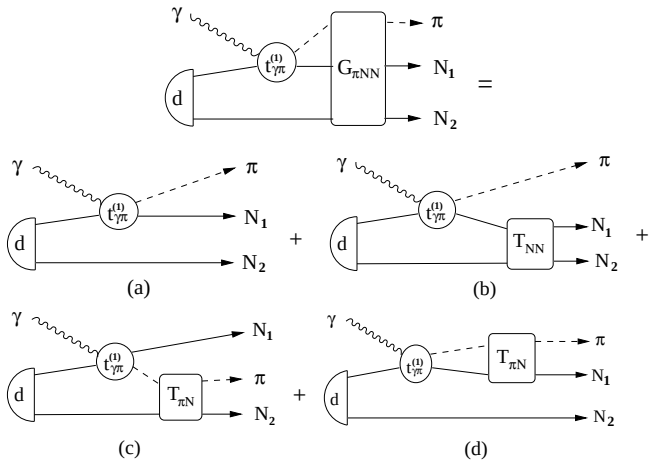

Fig. 3: Diagrammatic representation of the $\gamma d \to \pi NN$ amplitude including rescattering contributions in the two-body subsystems and neglecting all contributions of two-body meson-exchange currents. Diagram (a): impulse approximation (IA); (b), (c) and (d) "driving terms" from NN- and πN-rescattering, respectively. Diagrams when the elementary pion photoproduction operator acts on nucleon '2' are not shown in the figure but are included in the calculations. In the calculations, each diagram shown in the figure goes accompanied by the diagram obtained by the exchange $N_1 \leftrightarrow N_2$.

current $\mathbf{J}_{\gamma\pi}$ between the initial deuteron and the final πNN states. In a general frame, it is given by

$$T_{sm\mu m_d}(q,\Omega_\pi,\Omega_p) = -^{(-)}\langle \mathbf{q},\mathbf{p};\, sm|\varepsilon_\mu\cdot\mathbf{J}_{\gamma\pi}(0)|\mathbf{d};\,1\,m_d\rangle . \tag{20}$$

Introducing a partial wave decomposition, one finds for the scattering matrix the relation

$$T_{sm\mu m_d}(\Omega_\pi,\Omega_p) = e^{i(\mu+m_d-m)\phi_\pi}\, t_{sm\mu m_d}(\theta_\pi,\theta_p,\phi_{p\pi}) , \tag{21}$$

where $\phi_{p\pi} = \phi_p - \phi_\pi$. The small t-matrix depends only on θ_π, θ_p, and the relative azimuthal angle $\phi_{p\pi}$. The elements of this t-matrix are the basic quantities which determine unpolarized differential cross section and spin asymmetries. If parity is conserved, the following symmetry relation holds

$$t_{s-m-\mu-m_d}(\theta_\pi,\theta_p,\phi_{p\pi}) = (-)^{s+m+\mu+m_d}\, t_{sm\mu m_d}(\theta_\pi,\theta_p,-\phi_{p\pi}) \tag{22}$$

which leads to a corresponding relation for the $T_{sm\mu m_d}$-matrix

$$T_{s-m-\mu-m_d}(\theta_p,\phi_p,\theta_\pi,\phi_\pi) = (-)^{s+m+\mu+m_d}\, T_{sm\mu m_d}(\theta_p,-\phi_p,\theta_\pi,-\phi_\pi) . \tag{23}$$

Figure (3) shows the diagrammatic representation of the scattering matrix, where the elementary pion photoproduction operator acts on nucleon '1' only. All possible diagrams when the production operator acts on

nucleon '2' are not shown in this figure but are included in the calculations. In addition, all contributions of two-body currents are not displayed in Fig. (3). In principle, the full treatment of all interaction effects requires a full unitary πNN three-body calculation. In the present work, however, we will restrict ourselves to the inclusion of complete rescattering in the various two-body subsystems of the final state (diagrams (b), (c), and (d) in Fig. (3)).

For the calculation of the $T_{sm\mu m_d}$-matrix we start from the IA (diagram (a) in Fig. (3)) to which the contributions from NN- and πN-rescattering (diagrams (b), (c), and (d), respectively) are added. Then, the $T_{sm\mu m_d}$-matrix is given by the sum

$$T_{sm\mu m_d} = T^{IA}_{sm\mu m_d} + T^{NN}_{sm\mu m_d} + T^{\pi N}_{sm\mu m_d}\,. \tag{24}$$

In the following we briefly review these terms in some detail.

3.2.1 The impulse approximation

For the IA contribution (diagram (a) in Fig. (3)), which describes the production on one nucleon while the other acts as a spectator, one has

$$\begin{aligned} T^{IA}_{sm\mu m_d} =& \langle \mathbf{q},\mathbf{p},\, sm\,|\,[t^{(1)}_{\gamma\pi} + t^{(2)}_{\gamma\pi}]\,|\,1\,m_d\rangle \\ =& \sum_{m'}[\langle sm\,|\langle \mathbf{p}_1|t^{(1)}_{\gamma\pi}(W_{\gamma N_1})|-\mathbf{p}_2\rangle \phi_{m'm_d}(\mathbf{p}_2)|\,1\,m'\rangle \\ & - (1\leftrightarrow 2)]\,, \end{aligned} \tag{25}$$

where $t^{(1)}_{\gamma\pi}$ and $t^{(2)}_{\gamma\pi}$ denote the elementary pion photoproduction operator from nucleon '1' and '2', respectively, $W_{\gamma N_{1/2}}$ the invariant energy of the $\gamma N_{1/2}$ system, $\mathbf{p}_{1/2} = (\mathbf{k}-\mathbf{q})/2 \pm \mathbf{p}$, and $\phi_{mm_d}(\mathbf{p})$ is related to the internal deuteron wave function in momentum space by

$$\phi_{mm_d}(\mathbf{p}) = \sum_{L=0,2}\sum_{m_L} i^L (Lm_L\,1m|1m_d) u_L(p) Y_{Lm_L}(\hat{p})\,, \tag{26}$$

where $u_0(p)$ and $u_2(p)$ are the S and D components of the deuteron wave function, for which the realistic Paris potential model [39] is used.

3.2.2 The NN-rescattering

The NN transition matrix element (see diagram (b) in Fig. (3)) has the form

$$\begin{aligned} T^{NN}_{sm\mu m_d}(\mathbf{k},\mathbf{q},\mathbf{p}_1,\mathbf{p}_2) =& \sum_{m'}\int d^3\mathbf{p}'_{NN}\sqrt{\frac{E_1E_2}{E'_1E'_2}} \\ & \times \widetilde{\mathscr{R}}^{NN,t\mu}_{smm'}(W_{NN},\mathbf{p}_{NN},\mathbf{p}'_{NN})\frac{M_N}{\widetilde{p}^2 - p'^2_{NN} + i\varepsilon} \\ & \times T^{IA}_{sm'\mu m_d}(\mathbf{k},\mathbf{q},\mathbf{p}'_1,\mathbf{p}'_2)\,. \end{aligned} \tag{27}$$

The conventional NN-scattering matrix $\widetilde{\mathscr{R}}^{NN,t\mu}_{smm'}$ is introduced with respect to noncovariantly normalized states. It is expanded in terms of the partial wave contributions $\mathscr{T}^{NN,t\mu}_{Js\ell\ell'}$ as follows

$$\begin{aligned} & \widetilde{\mathscr{R}}^{NN,t\mu}_{smm'}(W_{NN},\mathbf{p}_{NN},\mathbf{p}'_{NN}) = \\ & \sum_J\sum_{\ell\ell'} \mathscr{F}^{NN,Js}_{\ell\ell' mm'}(\hat{p}_{NN},\hat{p}'_{NN})\mathscr{T}^{NN,t\mu}_{Js\ell\ell'}(W_{NN},p_{NN},p'_{NN})\,, \end{aligned} \tag{28}$$

where the purely angular function $\mathscr{F}^{NN,Js}_{\ell\ell' mm'}(\hat{p}_{NN},\hat{p}'_{NN})$ is defined by

$$\begin{aligned} & \mathscr{F}^{NN,Js}_{\ell\ell' mm'}(\hat{p}_{NN},\hat{p}'_{NN}) = \\ & \sum_M\sum_{m_\ell m_{\ell'}} C^{\ell sJ}_{m_\ell mM} C^{\ell' sJ}_{m_{\ell'}m'M} Y^\star_{\ell m_\ell}(\hat{p}_{NN}) Y_{\ell' m_{\ell'}}(\hat{p}'_{NN})\,. \end{aligned} \tag{29}$$

The necessary half-off-shell NN-scattering matrix $\mathscr{T}^{NN,t\mu}_{Js\ell\ell'}$ was obtained from separable representation of a realistic NN-interaction [37]. Explicitly, all S, P, and D waves were included in the NN-scattering matrix.

3.2.3 The πN-rescattering

For the contribution of πN-rescattering, two terms are considered. The diagrammatic representation of these terms are given by diagrams (c) and (d) in Fig. (3).

The πN transition matrix element of diagram (c) has the form

$$\begin{aligned} & T^{\pi N\,(c)}_{sm\mu m_d}(\mathbf{k},\mathbf{q},\mathbf{p}_1,\mathbf{p}_2) = \\ & \frac{1}{2}\sum_{\alpha'}\int d^3\mathbf{p}'_2\sqrt{\frac{\omega_q E_2}{\omega_{q'}E'_2}}\sum_{m_2m'_2}\sum_{\mu_2\mu'_2}\sum_{\tilde{t}\tilde{\mu}} \mathscr{C}^{\tilde{t}\tilde{\mu}}_{\alpha\alpha'}(m_2,m'_2,\mu_2,\mu'_2) \\ & \times\Big[\sum_{J\ell}\mathscr{F}^{\pi N}_{J\ell m_2m'_2}(\hat{p}_{\pi N},\hat{p}'_{\pi N})\mathscr{T}^{\pi N,\tilde{t}\tilde{\mu}}_{J\ell}(W_{\pi N}(\mathbf{p}_2),p_{\pi N},p'_{\pi N}) \\ & \times \mathscr{G}^{\pi NN(+)}_{0\,\pi N}(E_{\gamma d},\mathbf{q}',\mathbf{p}_1,\mathbf{p}'_2)\,T^{IA}_{s'm'\mu'm_d}(\mathbf{k},\mathbf{q}',\mathbf{p}_1,\mathbf{p}'_2) \\ & \times -(-)^{s+t}(\mathbf{p}_1\leftrightarrow\mathbf{p}_2)\Big]\,, \end{aligned} \tag{30}$$

with

$$\begin{aligned} & \mathscr{C}^{\tilde{t}\tilde{\mu}}_{\alpha\alpha'}(m_2,m'_2,\mu_2,\mu'_2) = C^{1\frac{1}{2}\tilde{t}}_{\mu\mu_2\tilde{\mu}} C^{1\frac{1}{2}\tilde{t}}_{\mu'\mu'_2\tilde{\mu}} \\ & \times \sum_{m_1} C^{\frac{1}{2}\frac{1}{2}s}_{m_1m_2m} C^{\frac{1}{2}\frac{1}{2}s}_{m_1m'_2m'} \sum_{\mu_1} C^{\frac{1}{2}\frac{1}{2}t}_{\mu_1\mu_2-\mu} C^{\frac{1}{2}\frac{1}{2}t'}_{\mu_1\mu'_2-\mu'}\,, \end{aligned} \tag{31}$$

and

$$\begin{aligned} \mathscr{F}^{\pi N}_{J\ell m_2m'_2}(\hat{p}_{\pi N},\hat{p}'_{\pi N}) =& \sum_{m_\ell m'_\ell M} C^{\frac{1}{2}\ell J}_{m_2m_\ell M} C^{\frac{1}{2}\ell J}_{m'_2m'_\ell M} \\ & \times Y^\star_{\ell m_\ell}(\hat{p}_{\pi N}) Y_{\ell m'_\ell}(\hat{p}'_{\pi N})\,, \end{aligned} \tag{32}$$

where $\alpha = (smt - \mu)$ and $\tilde{t}$ denotes the total isospin of the interacting pion and nucleon. The relative momentum of the final (initial) πN-subsystem is given by

$$\mathbf{p}_{\pi N} = \frac{M_N \mathbf{q} - m_\pi \mathbf{p}_2}{M_N + m_\pi}, \quad \mathbf{p}'_{\pi N} = \frac{M_N \mathbf{q}' - m_\pi \mathbf{p}'_2}{M_N + m_\pi}, \tag{33}$$

where $\mathbf{q}' = \mathbf{q} + \mathbf{p}_2 - \mathbf{p}'_2$.

Analogous to diagram (c), the πN matrix element of diagram (d) is given by

$$\begin{aligned} &T^{\pi N\,(d)}_{sm\mu m_d}(\mathbf{k},\mathbf{q},\mathbf{p}_1,\mathbf{p}_2) = \\ &\frac{1}{2}\sum_{\alpha'}\int d^3\mathbf{p}''_1 \sqrt{\frac{\omega_q E_1}{\omega_{q''} E''_1}} \sum_{m_1 m'_1}\sum_{\mu_1\mu'_1}\sum_{\tilde{t}\tilde{\mu}} \mathscr{C}^{\tilde{t}\tilde{\mu}}_{\alpha\alpha'}(m_1,m'_1,\mu_1,\mu'_1) \\ &\quad\times\Big[\sum_{J\ell}\mathscr{F}^{\pi N}_{J\ell m_1 m'_1}(\hat{\tilde{p}}_{\pi N},\hat{\tilde{p}}'_{\pi N}) \\ &\quad\times\mathscr{T}^{\pi N,\tilde{t}\tilde{\mu}}_{J\ell}(W_{\pi N}(\mathbf{p}_1),\tilde{p}_{\pi N},\tilde{p}'_{\pi N}) \\ &\times\mathscr{G}^{\pi NN(+)}_{0\,\pi N}(E_{\gamma d},\mathbf{q}'',\mathbf{p}_2,\mathbf{p}''_1) \\ &\quad\times T^{IA}_{s'm'\mu'm_d}(\mathbf{k},\mathbf{q}'',\mathbf{p}_2,\mathbf{p}''_1) - (-)^{s+t}(\mathbf{p}_1\leftrightarrow\mathbf{p}_2)\Big], \end{aligned} \tag{34}$$

where the relative momentum of the final (initial) πN-subsystem is given in this case by

$$\tilde{\mathbf{p}}_{\pi N} = \frac{M_N \mathbf{q} - m_\pi \mathbf{p}_1}{M_N + m_\pi}, \quad \tilde{\mathbf{p}}'_{\pi N} = \frac{M_N \mathbf{q}'' - m_\pi \mathbf{p}''_1}{M_N + m_\pi}, \tag{35}$$

with $\mathbf{q}'' = \mathbf{k} - \mathbf{p}_2 - \mathbf{p}''_1$.

Then the contribution from πN-rescattering of both diagrams (c) and (d) in Fig. (3) is given by

$$T^{\pi N}_{sm\mu m_d} = T^{\pi N\,(c)}_{sm\mu m_d} + T^{\pi N\,(d)}_{sm\mu m_d}. \tag{36}$$

The half-off-shell partial wave amplitudes $\mathscr{T}^{\pi N,\tilde{t}\tilde{\mu}}_{J\ell}$ in Eqs. (30) and (34) were found for the S, P, and D partial waves by numerical solution of the LS-equation. In the present calculations, these amplitudes are obtained from the separable energy-dependent πN potential presented in [38].

3.3 Definition of polarization observables

The cross section for arbitrary polarized photons and initial deuterons can be computed for a given t-matrix by applying the density matrix formalism similar to that given for deuteron photodisintegration [40]. The most general expression for all possible polarization observables is given by

$$\begin{aligned} \mathscr{O} = &\sum_{\alpha\alpha'}\int d\Omega_p\,\rho_s\, t^{\star}_{s'm'\mu'm'_d}\,\Omega_{s'm'sm}\,t_{sm\mu m_d} \\ &\times\rho^{\gamma}_{\mu\mu'}\,\rho^{d}_{m_d m'_d}, \end{aligned} \tag{37}$$

where $\rho^{\gamma}_{\mu\mu'}$ and $\rho^{d}_{m_d m'_d}$ denote the density matrices of initial photon polarization and deuteron orientation, respectively, $\Omega_{s'm'sm}$ is an operator associated with the observable, which acts in the two-nucleon spin space and ρ_s is a phase space factor. For further details we refer to Refs. [40,41].

As shown in Refs. [16,17,18,23] all possible polarization observables for the pion photoproduction reaction from the deuteron can be expressed in terms of the quantities

$$\begin{aligned} V^{\mu}_{IM}(q,\theta_\pi) = &\sqrt{\frac{2I+1}{3}}\int d\Omega_p\,\rho_s(E_\gamma,q,\Omega_\pi,\Omega_p) \\ &\times\sum_{m_d m'_d}(-)^{1-m_d}\begin{pmatrix}1 & 1 & I\\ m'_d & -m_d & M\end{pmatrix} \\ &\times\sum_{sm} t^{*}_{sm\mu m'_d}(q,\theta_\pi,\theta_p,\phi_{p\pi}) \\ &\times t_{sm\mu m_d}(q,\theta_\pi,\theta_p,\phi_{p\pi}), \end{aligned} \tag{38}$$

and

$$\begin{aligned} W_{IM}(q,\theta_\pi) = &\sqrt{\frac{2I+1}{3}}\int d\Omega_p\,\rho_s(E_\gamma,q,\Omega_\pi,\Omega_p) \\ &\times\sum_{m_d m'_d}(-)^{1-m_d}\begin{pmatrix}1 & 1 & I\\ m'_d & -m_d & M\end{pmatrix} \\ &\times\sum_{sm} t^{*}_{sm-1m'_d}(q,\theta_\pi,\theta_p,\phi_{p\pi}) \\ &\times t_{sm1m_d}(q,\theta_\pi,\theta_p,\phi_{p\pi}), \end{aligned} \tag{39}$$

where we use the convention of Edmonds [42] for the Wigner $3j$-symbols.

The unpolarized cross section is given by

$$\frac{d^3\sigma}{dqd\Omega_\pi} = V^1_{00}(q,\theta_\pi). \tag{40}$$

The photon asymmetry for linearly polarized photons is given by

$$\Sigma\,\frac{d^3\sigma}{dqd\Omega_\pi} = -W_{00}. \tag{41}$$

The vector and tensor target asymmetries are given by

$$T_{IM}\,\frac{d^3\sigma}{dqd\Omega_\pi} = (2-\delta_{M0})\,\Re e\,[i^I V^1_{IM}(q,\theta_\pi)]. \tag{42}$$

The photon and target double polarization asymmetries are given by
(i) Circular asymmetries:

$$T^c_{IM}\,\frac{d^3\sigma}{dqd\Omega_\pi} = -(2-\delta_{M0})\,\Im m\,[i^I V^1_{IM}(q,\theta_\pi)]. \tag{43}$$

(ii) Longitudinal asymmetries:

$$T^l_{IM}\,\frac{d^3\sigma}{dqd\Omega_\pi} = -i^I W_{IM}(q,\theta_\pi). \tag{44}$$

4 Results and discussion

The discussion of our results is divided into four parts as follows:

- First, we will discuss various polarization observables for incoherent pion photoproduction from the deuteron in the $\Delta(1232)$-resonance region. Numerical results for the three isospin channels of the $d(\gamma,\pi)NN$ reaction will be given. The $\gamma d \to \pi NN$ scattering amplitude is given as a linear combination of the on-shell matrix elements of pion photoproduction on the two nucleons (diagram (a) in Fig. (3)). The results of this part are obtained with the deuteron wave function of the Paris potential [39] and the elementary pion production operator on the free nucleon of Schmidt *et al.* [6] which describes well the $\gamma N \to \pi N$ reaction channels (see Ref. [22] in which we have presented results for the helicity dependence of the $\gamma\mathbf{N} \to \pi N$ reaction channels in comparison with the recent experimental data from the GDH Collaboration [43].).
- In the second part, the influence of final-state NN interaction (diagram (b) in Fig. (3)) in various polarization observables for the reaction $\gamma d \to \pi^- pp$ will be studied. The understanding of this mechanism is of great importance to understand the basic NN interaction. The second point of interest is to analyze the preliminary experimental data for the differential polarized cross-section difference for parallel and antiparallel helicity states from [12] and for the linear photon asymmetry from LEGS [14] in order to keep up with the development of the experimental data. For nucleon-nucleon scattering in the NN-subsystem, we use a specific class of separable potentials [37] which historically have played and still play a major role in the development of few-body physics and also fit the phase shift data for NN-scattering. This separable model is most widely used in the case of the πNN system (see, for example, Ref. [44] and references therein).
- In the third part, we will present and discuss results for total cross section and various polarization observables when in addition to the pure IA (diagram (a) in Fig. (3)) and NN-FSI (diagram (b) in Fig. (3)), the πN-rescattering (diagrams (c) and (d) in Fig. (3)) is also included. Results for the three isospin channels of the $d(\gamma,\pi)NN$ reaction will be given in the energy region from π-threshold up to the $\Delta(1232)$-resonance. Extension of our previous works [17,18,19,20,21] to the π-threshold region is presented in order to understand the dynamics of the pion photoproduction amplitude near π-threshold. For this purpose, a more realistic elementary amplitude from Ref. [31] is used which allows to provide a more realistic description of the π-threshold region. For both NN- and πN-scattering in the two-body subsystems, we use separable representations of realistic potentials from Refs. [37,**?**]. The total cross section, the doubly polarized cross sections for the parallel and antiparallel helicity states, the spin response of the deuteron, i.e., the asymmetry of the total photoabsorption cross section with respect to parallel and antiparallel spins of photon and deuteron, the linear photon asymmetry, target asymmetries, the beam-target double polarization E-asymmetry, and the deuteron GDH integral will be discussed in this part.
- The last part is devoted to study the sensitivity of the results for total cross section and polarization observables to the elementary pion photoproduction operator on the free nucleon.

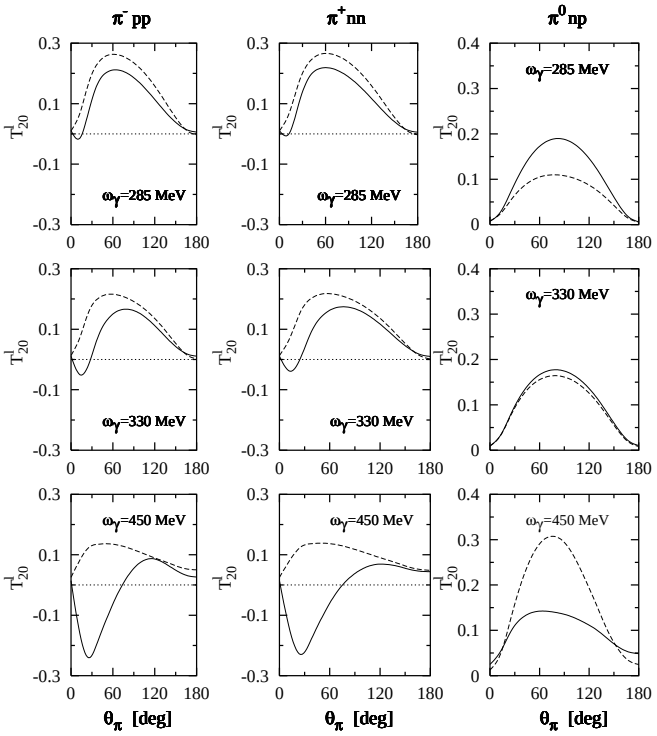

Fig. 4: The double polarization asymmetry T_{20}^{ℓ} of $\mathbf{d}(\gamma,\pi)NN$ channels as a function of pion angle θ_π at various photon lab-energies. The solid curves show the results of the IA-calculation while the dotted curves represent the results when only the $\Delta(1232)$-resonance is taken into account. The left, middle and right panels represent the results for $\gamma d \to \pi^- pp$, $\pi^+ nn$ and $\pi^0 np$, respectively.

4.1 The impulse approximation

We start the discussion with a sample of results for the longitudinal double polarization asymmetry T_{20}^{ℓ} which are

plotted in Fig. (4) as a function of emission pion angle θ_π at various photon lab-energies for all the three charge states of the pion for the reaction $\gamma\mathbf{d} \to \pi NN$ (see also Ref. [17]). For neutral pion production (see the right panels of Fig. (4)), we see that T_{20}^{ℓ} has always positive values for all photon lab-energies and emission pion angles. For energies below and above the $\Delta(1232)$-resonance, the double polarization asymmetry T_{20}^{ℓ} shows sensitivity on the Born terms, in particular for angles between 60° and 120°. Furthermore, it is apparent that at extreme forward and backward emission pion angles the asymmetry T_{20}^{ℓ} is very small in comparison to other angles. At 450 MeV the dominant contribution comes from the resonance term. For the calculations of charged pion production channels (see the left and middle panels of Fig. (4)), we see that T_{20}^{ℓ} has negative values at forward pion angles which is not the case at backward angles. It is also noticeable that the contributions of Born terms are large, in particular at energies above the resonance region. At extreme backward angles, we see that T_{20}^{ℓ} has small positive values.

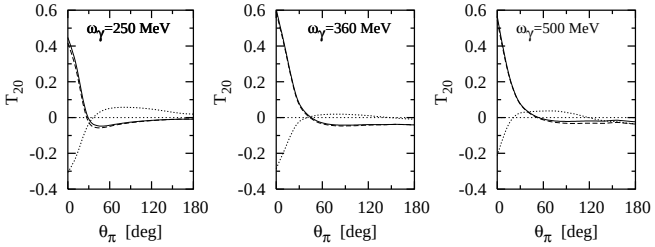

Fig. 5: Tensor target asymmetry T_{20} of $\mathbf{d}(\gamma,\pi)NN$ channels as a function of emission pion angle at various photon lab-energies. The solid, dashed, and dotted curves correspond to $\gamma d \to \pi^- pp$, $\pi^+ nn$, and $\pi^0 np$, respectively.

In Fig. (5) we present the results for the tensor target asymmetry T_{20} as a function of θ_π [18]. Predictions for the three isospin channels of $\mathbf{d}(\gamma,\pi)NN$ at various photon lab-energies are given. For the reaction $\gamma\mathbf{d} \to \pi NN$ at forward and backward emission pion angles, the asymmetry T_{20} allows one to draw specific conclusions about details of the reaction mechanism. Comparing with the results for linear photon and vector target asymmetries [17,18] we found that for charged pion production channels the asymmetry T_{20} has relatively large positive values at pion forward angles (at $\theta_\pi < 30°$) while small negative ones are found when θ_π changes from 30° to 180°. For neutral pion production channel, we see that T_{20} has negative values at forward angles and positive ones at backward angles. Only at energies above the Δ-region we observe small negative values at extreme backward angles.

The longitudinal double-polarization asymmetry T_{2+2}^{ℓ} is plotted in Fig. (6) as a function of pion angle for all the

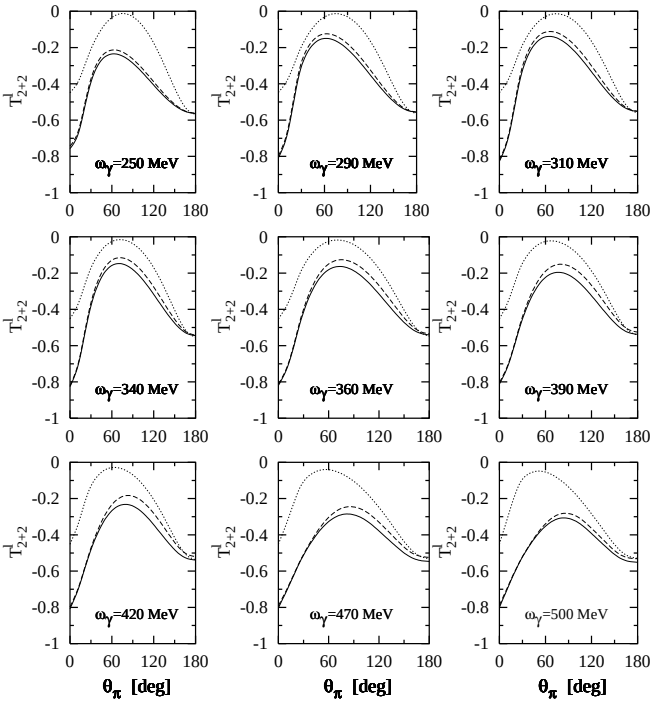

Fig. 6: The double-polarization asymmetry T_{2+2}^{ℓ} of $\mathbf{d}(\gamma,\pi)NN$ at various photon lab-energies. Notation as in Fig. (5).

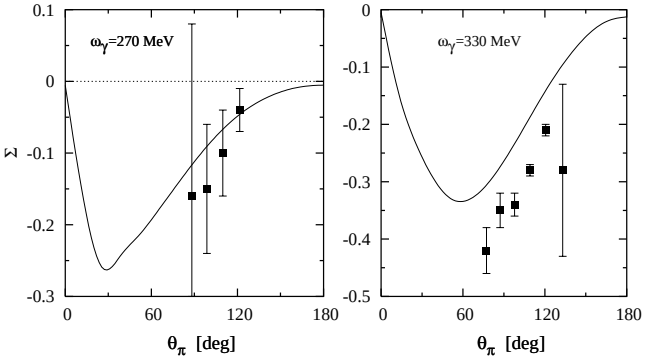

Fig. 7: Photon beam asymmetry Σ for $d(\gamma,\pi^-)pp$ reaction in comparison with the 'preliminary' experimental data from LEGS@BNL Collaboration [14].

three charge states of the pion for the reaction $\gamma\mathbf{d} \to \pi NN$ at various photon lab-energies (see also Ref. [18]). The solid, dashed, and dotted curves correspond to $\gamma\mathbf{d} \to \pi^- pp$, $\pi^+ nn$, and $\pi^0 np$, respectively. In general, one readily notes that the longitudinal asymmetry T_{2+2}^{ℓ} has negative values. For neutral and charged pion production channels, it is apparent that the asymmetry T_{2+2}^{ℓ} has qualitatively the same behavior. We see also that the values of T_{2+2}^{ℓ} for π^0 channel are greater (in absolute value smaller) than its values for $\pi^{\pm}$ channels, in particular at $\theta_\pi = 0°$. Furthermore, we noticed that the

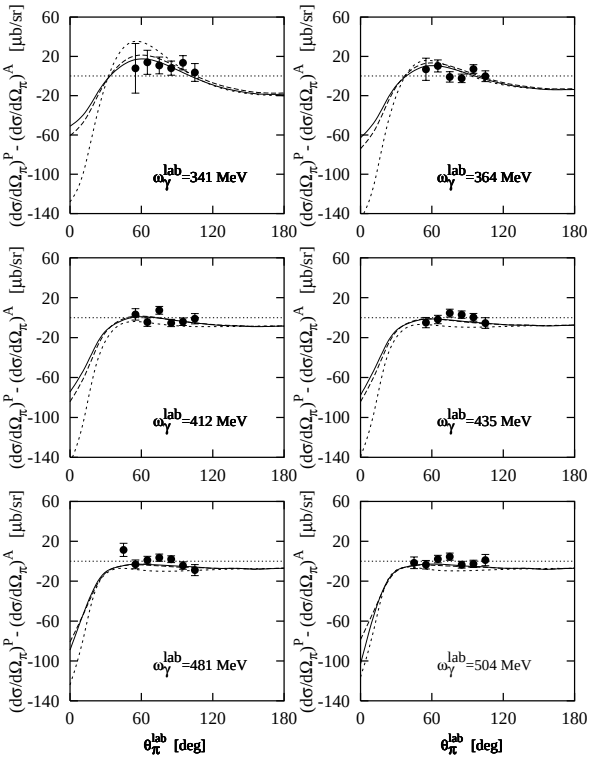

Fig. 8: The differential polarized cross-section difference $(d\sigma/d\Omega_\pi)^P - (d\sigma/d\Omega_\pi)^A$ for $\gamma\mathbf{d} \to \pi^- pp$ as a function of $\theta_\pi^{\rm lab}$ in comparison with experimental data from Ref. [12] at different photon lab-energies. Dashed curves: IA; solid curves: IA+*NN*-rescattering; dotted curves: predictions for $\gamma\mathbf{n} \to \pi^- p$ reaction.

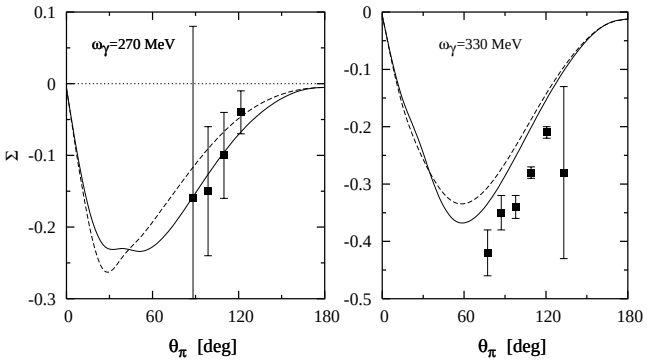

Fig. 9: Photon asymmetry Σ for the reaction $d(\gamma,\pi^-)pp$ at two different photon lab-energies in comparison with the preliminary data from LEGS [14]. Notation of curves: dashed: IA; solid: IA+*NN*-rescattering.

values of T_{2+2}^{ℓ} in the case of π^0-production are insensitive to the photon energy and/or pion angle, which is not the case for $\pi^{\pm}$-production channels. It is very interesting to examine these asymmetries experimentally.

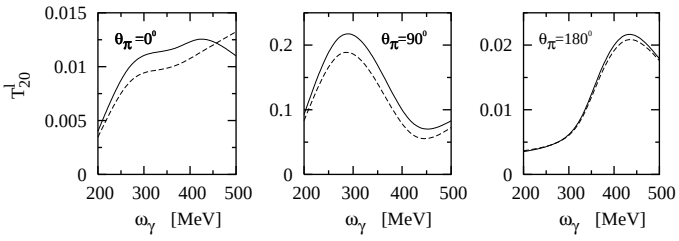

Fig. 10: The double-polarization asymmetry T_{20}^{ℓ} for $\mathbf{d}(\gamma,\pi^-)pp$ as a function of photon lab-energy at fixed values of θ_π. Notation as in Fig. (9).

The photon asymmetry Σ for linearly polarized photons is shown in Fig. (7) (see also Ref. [18]) in comparison with experimental data. In view of the fact that data for π^+ and π^0 production channels are not available, we concentrate the discussion on π^- production, for which we have taken the 'preliminary' experimental data from the LEGS@BNL Spin Collaboration [14]. In agreement with these preliminary data, one can see that the predictions in the pure IA can hardly provide a reasonable description of the data. Major discrepancies are evident which very likely come from the neglect of FSI effects. This means that the simple spectator approach cannot describe the experimental data.

4.2 Influence of NN final-state interaction

Here, we discuss the influence of the *NN*-FSI effect on polarization observables for the reaction $\gamma d \to \pi^- pp$ only. We begin the discussion by presenting the results for the differential polarized cross-section difference for parallel $(d\sigma/d\Omega_\pi)^P$ and antiparallel $(d\sigma/d\Omega_\pi)^A$ helicity states in pure IA and with *NN*-rescattering, as shown in Fig. (8) as a function of the emission pion angle in the laboratory frame at various photon lab-energies (see also Ref. [19]). It is readily seen that *NN*-rescattering - the difference between the dashed and the solid curves - is quite small, and indeed almost completely negligible at pion backward angles. The reason for this stems from the fact that in charged-pion production, $^3S_1$-contribution to the *NN* final state is forbidden.

By comparing the results for the difference $(d\sigma/d\Omega_\pi)^P - (d\sigma/d\Omega_\pi)^A$ in the case of $\gamma\mathbf{d} \to \pi^- pp$ (solid curves in Fig. (8)) with those in the case of the free reaction $\gamma\mathbf{n} \to \pi^- p$ (dotted curves in Fig. (8) and also presented in Ref. [22] in which we have investigated the helicity dependence of the $\gamma\mathbf{N} \to \pi N$ reaction channels), we see that a large correction is needed to go from the bound deuteron to the free neutron case [19]. The difference between the two results decreases to a tiny effect at backward angles. Figure (8) also gives a comparison of the results for the helicity difference with the experimental data from the GDH Collaboration [12].

It is obvious that quite satisfactory agreement with experiment is achieved [19]. An experimental check of the helicity difference at extreme forward and backward pion angles is needed. Also, an independent check in the framework of effective field theory would be very interesting.

Figure (9) shows a comparison of the numerical results for the linear photon asymmetry Σ in the pure IA (dashed curves) and with NN-rescattering (solid curves) [20] with the preliminary experimental data from the LEGS Spin Collaboration [14]. We see that the general feature of the data is reproduced. However, the discrepancy is rather significant in the region where the photon energy close to the Δ-resonance. In the same figure, we also show the results from the IA only (dashed curves). It is seen that the NN-rescattering yields an about 10% effect in the region of the peak position. We found that this is mainly due to the interference between the IA amplitude and the NN-FSI amplitude. In agreement with our results in the pure IA [18], one notes that the pure IA (dashed curves in Fig. (9)) cannot describe the experimental data. The inclusion of NN-FSI leads at 270 MeV to a quite satisfactory description of the data, whereas at 330 MeV the NN-FSI effect is small and therefore differences between theory and experiment are still evident. It is appear that our model is still not capable of describing the measured photon asymmetry, even if NN-FSI is included. The influence of NN-rescattering on the longitudinal double-spin asymmetry T_{20}^{ℓ} was investigated in our previous work [21] as a function of photon lab-energy for fixed angles (see Fig. (10)). We see that T_{20}^{ℓ} has very small values at forward pion angles around $\theta_\pi < 60^\circ$. These values increase (in absolute value decrease) with increasing the photon energy. At extreme backward angles, we see that T_{20}^{ℓ} has small positive values.

From the foregoing discussion for the polarized cross sections and spin asymmetries [19,20,21] it is apparent that the contribution of NN-FSI is much important in the energy region around the Δ-resonance, especially in the peak position and must be considered in the analysis of the forthcoming experiments. One notices that the inclusion of NN-FSI leads to an overestimation by about 10% of the plane wave results. For lower and higher energies, one can see that the NN-FSI effect is small. This means, in particular with respect to a test of theoretical models for pion production amplitudes on the neutron, that one needs a reliable description of the scattering process. Hopefully, these predictions can be tested in the near future when the data from the on-going experiments become available.

4.3 Effects of NN and πN-rescattering

The main goal of this section is to report on a theoretical prediction for the total cross section and spin observables for both the charged and neutral pion photoproduction channels of the reaction $\gamma d \to \pi NN$ in the energy region from π-threshold up to the $\Delta(1232)$-resonance [29,30]. We also disentangle the different contributions to the observables from the *bare* elementary reaction, the NN-rescattering, and the πN-rescattering. We are going to extend the work in the preceding papers [17,18,22,19,20,21] to the π-threshold region in order to understand the dynamics of pion photoproduction amplitude near π-threshold. The extension includes the following important aspects:

(i) A more realistic elementary pion photoproduction operator from Ref. [31] is used. This model based on an effective Lagrangian approach (ELA) includes seven nucleon resonances ($\Delta(1232)$, N(1440), N(1520), N(1535), $\Delta(1620)$, N(1650), and $\Delta(1700)$), in addition to Born and vector-meson exchange terms. It incorporates a new theoretical treatment of spin-3/2 resonances avoiding pathologies present in previous models and also allows to provide a more reliable description of the π-threshold region.

(ii) The influence of both NN- and πN-FSI effects on unpolarized cross sections and spin asymmetries is quantitatively studied. We consider, besides the pure impulse approximation (IA), complete rescattering in the final two-body subsystems, i.e. in the NN- and πN-subsystems.

(iii) Comparison with recent experimental data and other theoretical models is discussed.

We compare in the figures calculations with different ingredients, showing separately the contribution from the bare interaction and the final state interaction one. We call impulse approximation (IA) to the bare contribution to the observables shown in diagram (a) of Fig. (3) together with the same diagram exchanging $N_1 \leftrightarrow N_2$. In what follows, when we cite any diagram (a)-(c) in Fig. (3) we implicitly mean the contributions of both the depicted diagram and the corresponding one obtained under $N_1 \leftrightarrow N_2$ exchange.

We have to be careful with what we call IA. A truly IA calculation (a calculation that includes only diagram (a)) cannot employ directly the elementary amplitudes which fit the electromagnetic multipoles of $\gamma N \to \pi N$ process, because the effect of πN-rescattering is included in those fits. For example, if we use the multipoles provided by the ELA model which fit the experimental data, and afterwards we include πN-rescattering, we are not really including just diagram (a) + diagram (c), but rather diagram (a) + diagram (c) + diagram (c) calculation. Therefore, if we wish to calculate the contribution coming just from diagram (a), the bare contribution to the amplitude has to be extracted from the analysis of the $\gamma N \to \pi N$, where FSI has to be removed. This was done for instance in Ref. [31]. We name IA* to the calculations where the πN-rescattering is included in the elementary reaction. IA* is therefore equivalent to a diagram (a) + diagram (c) calculation. In section 4.4 we compare results for IA*+rescattering and IA+rescattering results using MAID and ELA models. We refer to the calculation that includes diagram (b) as NN and diagram

(c) using the πN rescattering, as πN. Therefore the full calculation, consistent and with all the effects considered in this work is what we refer as IA+$\pi N + NN$. Results in Refs. [23,24,25] contain a double-counting of the πN-rescattering because their starting point is MAID and SAID amplitudes as elementary reaction and afterwards they include πN-rescattering (they perform what we call an IA$^* + \pi N + NN$ calculation).

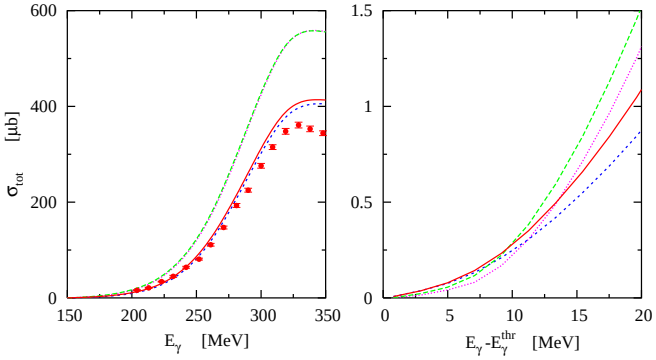

Fig. 11: Total cross section for $d(\gamma,\pi^0)np$ using the electromagnetic multipoles of set no. 2 from the effective Lagrangian approach [31]. Left panel: results from π-threshold up to the $\Delta(1232)$-resonance region in comparison with the experimental data from Krusche *et al.* [11]. Right panel: results near π-threshold as a function of the excess energy above π-threshold $E_\gamma - E_\gamma^{thr}$. Curve conventions: (dotted) IA; (long-dashed) IA+πN; (short-dashed) IA+NN; (solid) IA+$NN + \pi N$.

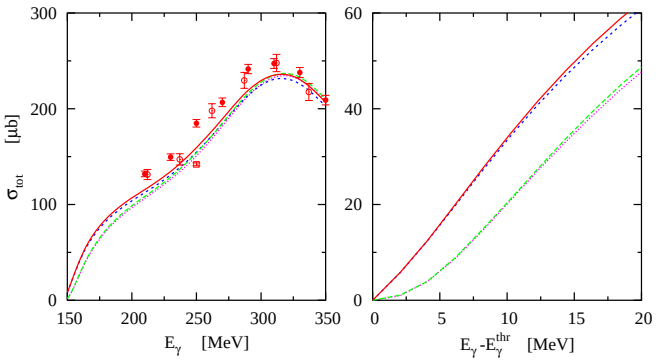

Fig. 12: Same as in Fig. (11) but for $d(\gamma,\pi^-)pp$. Experimental data from Benz *et al.* [45] (solid circles), Chiefari *et al.* [46] (open circles) and Quraan *et al.* [47] (open square).

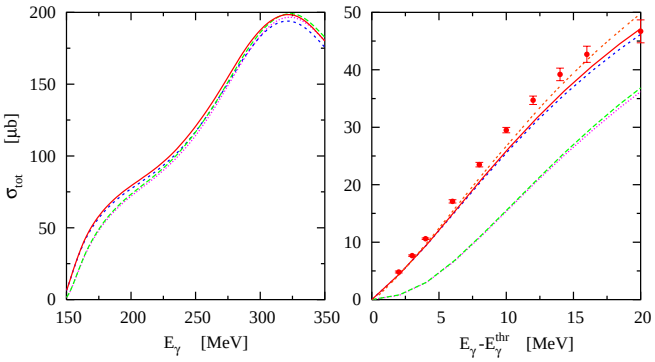

Fig. 13: Same as in Fig. (11) but for $d(\gamma,\pi^+)nn$. Experimental data are from Booth *et al.* [48]. The three-dashed curve in the right panel denotes the ChPT prediction of Lensky *et al.* [49].

4.3.1 Total cross sections

In the left panels of Figs. (11), (12), and (13) we show the results for the total cross section from π-threshold up to the $\Delta(1232)$-resonance region for the $\gamma d \to \pi^0 np$, $\gamma d \to \pi^- pp$, and $\gamma d \to \pi^+ nn$ reactions, respectively (see also Ref. [30]). In the right panels of the same figures our predictions for the region near π-threshold as function of the excess energy above π-threshold, $E_\gamma - E_\gamma^{thr}$, in the laboratory system, are also shown. From the comparison with the experimental data it stems that our model overestimates the total cross section for the π^0 channel and slightly underestimates it for the π^+ channel, however, on the overall, we obtain a very good agreement. Compared to the ChPT prediction from [49] for the π^+ production channel near π-threshold (right panel of Fig. (13)) a good agreement is obtained when FSI is included.

The importance of rescattering in the neutral channel is clearly addressed when the full calculation is compared to the IA one. It is very clear from the right panels in Figs. (11), (12), and (13) that the charged pion production cross-sections differ significantly in magnitude from the neutral pion ones due to the Kroll-Rudermann term (diagram (D) in Fig. (1)) which does not contribute to the neutral pion production reaction. We would like to emphasize that at photon energies close to π-threshold, almost all the contribution to the cross sections comes from Born terms. We observe also that the πN-rescattering is not very important in both neutral and charged channels in what regards to the total cross section and that the NN-rescattering plays a central role in neutral pion production but not so in charged pion channels. The result on charged pion production is compatible with what is obtained for the elementary process $\gamma N \to \pi N$ where the charged-production observables are already well predicted without the inclusion of final state interactions [31]. Since the contribution from πN-rescattering is small, the effect of multiple scattering of the pion with

two outgoing nucleons (see diagrams (d) and (e) in Fig. (3)) is expected to be small too (see also [50]).

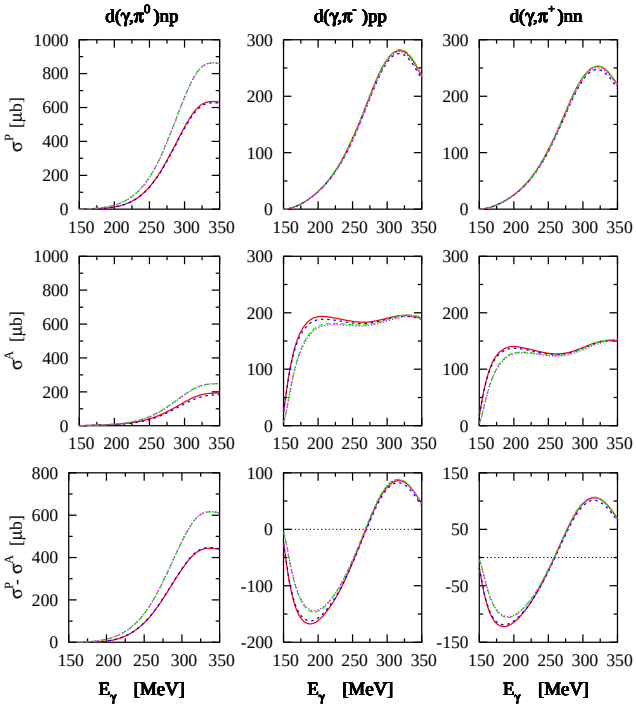

Fig. 14: The helicity dependent total photoabsorption cross sections for the separate channels of $\mathbf{d}(\gamma,\pi)NN$ for circularly polarized photons on a longitudinally polarized deuteron with spin parallel σ^P (upper panel) and antiparallel σ^A (middle panel) to the photon spin in the energy region from π-threshold up to the $\Delta(1232)$-resonance. The lower panel shows the difference $\sigma^P - \sigma^A$, i.e., the deuteron spin asymmetry of total photoabsorption cross section. Curve conventions as in Fig. (11).

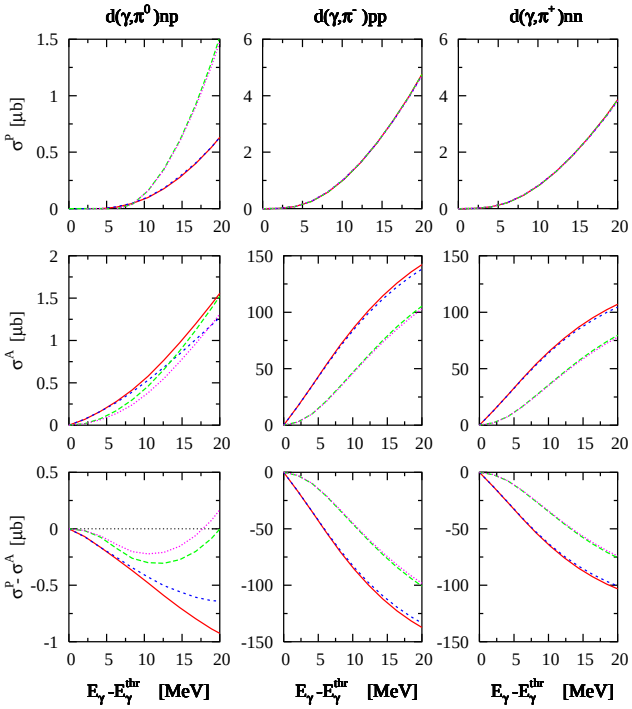

Fig. 15: Same as in Fig. (14) but in the energy region near π-threshold. $E_\gamma - E_\gamma^{thr}$ denotes the excess energy above π-threshold in the laboratory system.

4.3.2 Helicity dependent cross sections

The results for the doubly polarized total cross sections in the case of the IA alone and with FSI effects are shown in Fig. (14) (from π-threshold up to the $\Delta(1232)$-resonance region) and Fig. (15) (near π-threshold region) (see also Ref. [29]). Results are displayed in Figs. (14) and (15) as follows: (upper panel) total photoabsorption cross sections σ^P for circularly polarized photons on a target with spin parallel to the photon spin; (middle panel) σ^A, the same for antiparallel spins of photon and deuteron target; (lower panel) spin asymmetry $\sigma^P - \sigma^A$ for the individual contributions of the different pion charge states to the $\gamma\mathbf{d} \to \pi NN$ reaction. Several experiments to measure the deuteron spin asymmetry are presently underway [12]. In these experiments, deuterium serves as a neutron target and quasifree kinematics is preferred in order to minimize possible interaction effects.

Left panels in Figs. (14) and (15) show the importance of rescattering effects in the neutral channel when the full calculation (solid curve) is compared to the IA one (dotted curve). The most important contribution to FSI comes from NN-rescattering, whilst πN-rescattering is much smaller and is significative only in σ^A at photon energies close to π-threshold (see the left panel in Fig. (15)). This is due to the non-orthogonality of the final state plane wave in IA to the deuteron bound state wave function. We also find that FSI effects are equally important for both σ^P and σ^A. FSI effects lead to an overall strong reduction of the spin asymmetry in the energy region of the $\Delta(1232)$-resonance [29]. σ^P is larger than σ^A because of the $\Delta(1232)$-excitation.

The cross sections σ^P and σ^A as well as the spin asymmetry $\sigma^P - \sigma^A$ present qualitative and quantitatively similar behaviors for both charged pion production channels (see also Ref. [29]). The FSI effects appear mainly in σ^A at photon lab-energies close to π-threshold (Fig. (15)). We find that the spin asymmetry $\sigma^P - \sigma^A$ starts out negative due to the E_{0+} multipole, which is dominant in the π-threshold region, and has a strong positive contribution at higher energies due to the M_{1+} multipole, which is dominant in the $\Delta(1232)$-resonance region. The effect of FSI is important for both the neutral

and charged pion production channels in the π-threshold region.

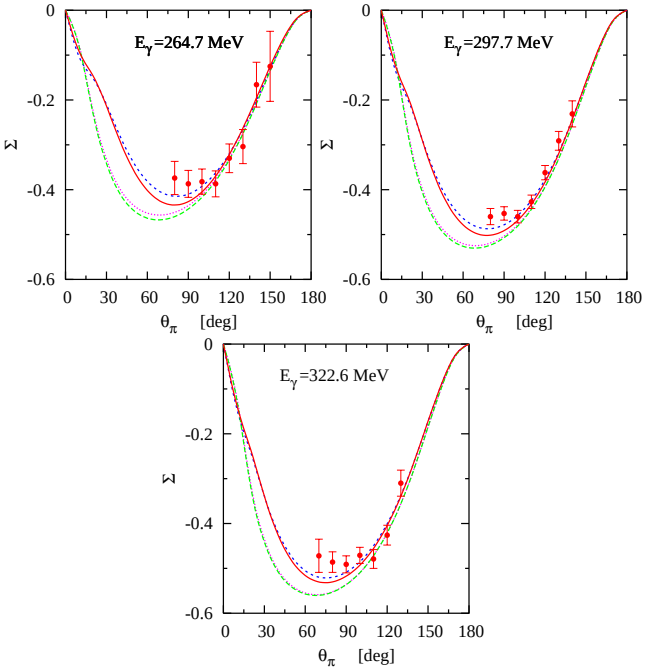

Fig. 16: The beam asymmetry Σ for linearly polarized photons for semi-exclusive π^0 photoproduction from the deuteron as a function of pion angle in the laboratory frame of the deuteron at different photon lab-energies using the electromagnetic multipoles of set no. 2 from the effective Lagrangian approach [31]. Curve conventions as in Fig. (11). Experimental data are from the LEGS Collaboration (LEGS-exp-L3b) [14].

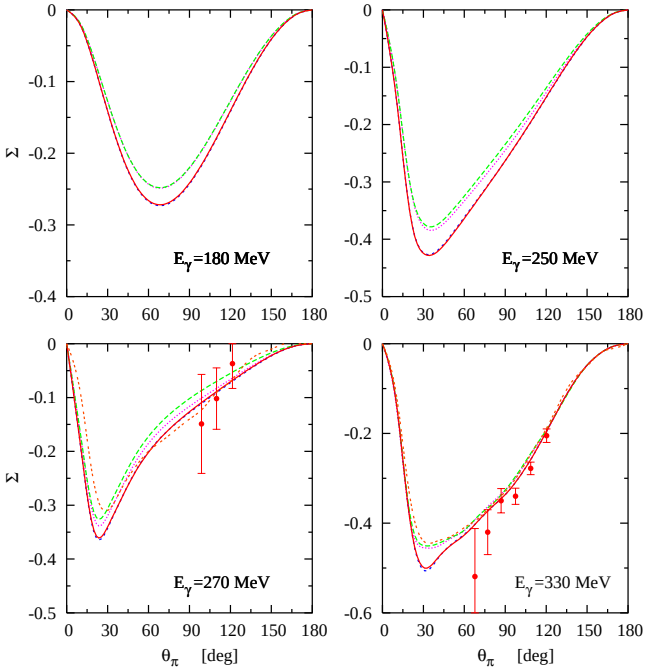

Fig. 17: Same as in Fig. (16) but for the $\gamma d \to \pi^- pp$ channel. The three-dashed curves in the bottom panels denote the results of Lee and Sato [51] without FSI effects. Experimental data are from the LEGS Collaboration (LEGS-exp-L3b) [14].

4.3.3 Beam asymmetry

In Figs. (16) and (17) we show a sample of our results for the photon beam asymmetry Σ for π^0 and π^- channels, respectively (see Ref. [29]). This asymmetry does not exhibit a strong effect of the rescattering contribution and it is an excellent test of any weaknesses in the underlying elementary reaction model.

The first effect that we observe is that πN-rescattering contribution is small for this observable in the energy region under study. The influence of FSI is noticeable at the lowest energy and forward pion angles. With increasing photon lab-energy the effect of FSI becomes smaller although not negligible, even at the highest energy. In Fig. (17) we show our results for π^- production together with the Lee-Sato calculation [51] which is equivalent to our IA* calculation but using the dynamical model developed in [52]. The Sato and Lee model provides a result close to the one from our model except at the small angles region, where a sizeable deviation at 30 degrees is observed due to rescattering contributions. The small angle region is sensitive to model dependencies and rescattering effects and the results are again more dependent on the NN-rescattering than on the πN-rescattering. The NN-rescattering tends to enlarge the asymmetry in charged channels and to decrease its value slightly in the neutral channel.

When compared to the recent model by Levchuk *et al.* [25] our results seem to compare better to the data from LEGS (LEGS-exp-L3b) [14], Figs. (16) and (17), but we have to wait until the final data are available to make a final statement on this comparison.

4.3.4 Target asymmetries

The target asymmetries T_{22}, T_{21}, and T_{20} for the neutral channel are plotted in Fig. (18) (see also Ref. [30]). These asymmetries show a large effect on the rescattering contribution and the employed elementary reaction model. Thus, they constitute an excellent set of observables to test our model and to compare it to other models. Actually, our predictions for these observables are quite different from those by Levchuk *et al.* [25] and by Arenhövel and Fix [23]. Unfortunately no data are currently available for these observables and therefore we cannot make a comparison to experimental data.

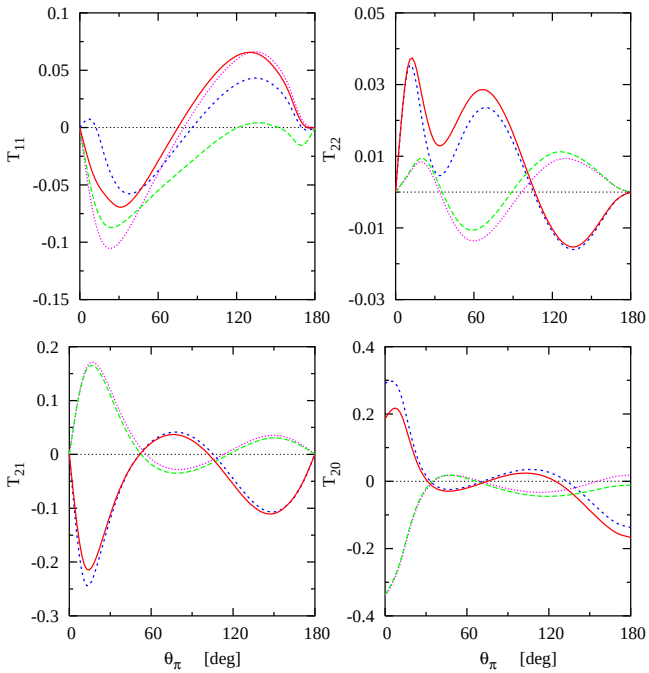

Fig. 18: Target asymmetries T_{11}, T_{22}, T_{21}, and T_{20} for semiexclusive π^0 photoproduction from the deuteron at photon lab-energy $E_\gamma = 265$ MeV using the electromagnetic multipoles of set no. 2 from the effective Lagrangian approach [31]. Curve conventions as in Fig. (11).

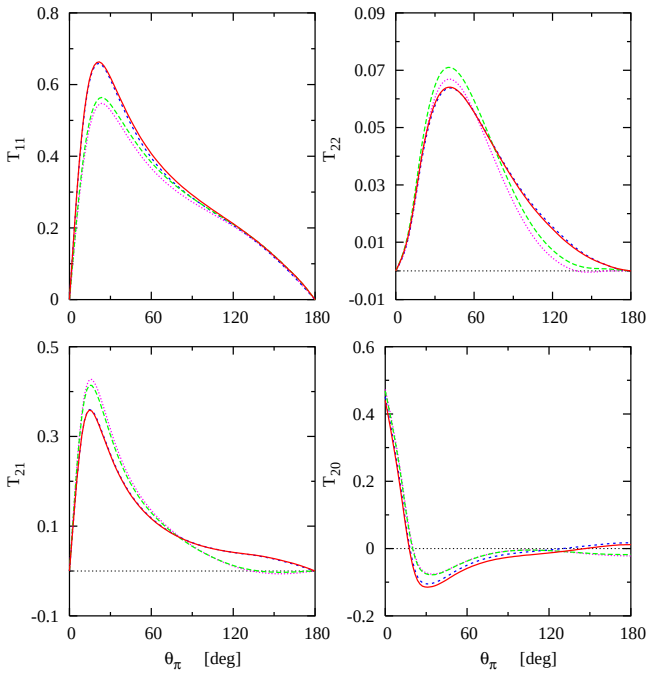

Fig. 19: Same as in Fig. (18) but for $\gamma d \to \pi^- pp$ at photon lab-energy $E_\gamma = 270$ MeV.

In charged channels (see Fig. (19)) the structure of the target asymmetries T_{22}, T_{21}, and T_{20} is very simple. They all present a peak at a certain angle (T_{11}, T_{22}, and T_{21} approximately between 25 and 60 degrees, and T_{20} at zero degrees) with a decreasing asymmetry towards zero for 180 degrees except for the T_{20} asymmetry and low-energy T_{11}. We find that πN-rescattering effects are negligible. Our results for the π^- channel are similar to the ones of Levchuk *et al.* [25] probably due to the fact that final state interactions are not so important in charged channels. However, the T_{21} asymmetry we calculate behaves in a different way than those of Refs. [23,25] in the large angle region and seems to have some model dependency (see Figs. (9) in [23] and (21) in [25]).

4.3.5 The double polarization E-asymmetry

There is a great deal of interest in experiments [14] to determine the beam-target double polarization E-asymmetry for the $\gamma\mathbf{d} \to \pi NN$ reaction channels. In connection with this study, we provide in Fig. (20) a sample of E-asymmetry as a function of the emission pion angle θ_π in the laboratory frame for the individual pion photoproduction channels (see also Ref. [29]). This asymmetry is given by

$$E(\theta_\pi) = \frac{d(\sigma^A - \sigma^P)/d\Omega}{d(\sigma^A + \sigma^P)/d\Omega} = \frac{d(\sigma^A - \sigma^P)/d\Omega}{2(d\sigma_0/d\Omega)}, \qquad (45)$$

where $d\sigma^P/d\Omega$ and $d\sigma^A/d\Omega$ represent the spin parallel and antiparallel differential cross sections, respectively, and $d\sigma_0/d\Omega$ denotes the unpolarized differential cross section. The helicity dependent cross sections are well suited to verify the GDH sum rule, to do partial channel analysis, and to give contributions to the double polarization E-asymmetry. This asymmetry appears as an interference between the amplitudes with different parity-exchange properties.

The helicity E-asymmetry (Fig. (20)) has qualitatively a similar behavior for all pion photoproduction channels. The maximum value of E equals unity at $\theta_\pi = 0^\circ$ and 180°. The curves begin with unity and decrease as the pion angle increases until the minimum value is reached at $\theta_\pi \simeq 90^\circ$. Then, it increases again to unity. The negative values in the E-asymmetry come mainly from higher positive contribution in $d\sigma^P/d\Omega$ [29].

Figure (20) shows also that the helicity E-asymmetry does not exhibit a strong effect of the rescattering contribution and, therefore, it is an excellent observable to test any weakness in the underlying elementary reaction model. We find that FSI are sizeable in the neutral channel, whereas in charged channels they are noticeable only at the lowest energy. The E-asymmetry proves to be sensitive to the choice of the input elementary $\gamma N \to \pi N$

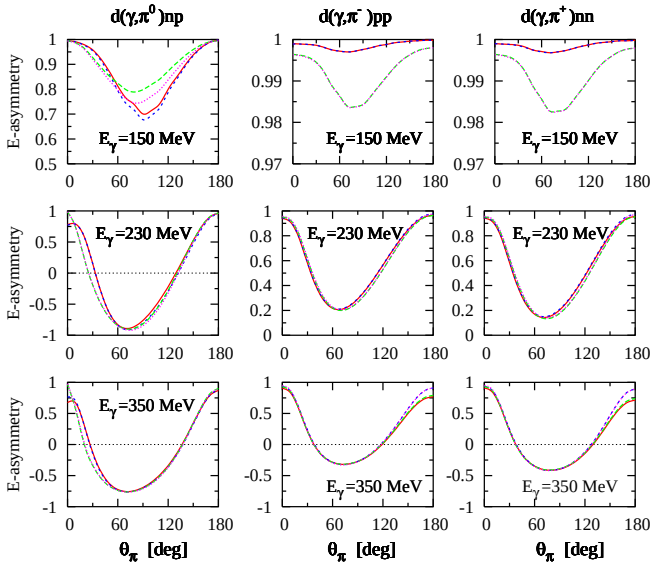

Fig. 20: The double polarization E-asymmetry (see Eq. (45) for its definition) as a function of the pion angle in the laboratory frame at various photon lab-energies for the separate channels of the reaction $\mathbf{d}(\gamma,\pi)NN$ for circularly polarized photons on a longitudinally polarized deuteron. Curve conventions as in Fig. (11).

amplitude and to the double-counting of the πN-rescattering [29]. We would like to point out that very preliminary data for the helicity E-asymmetry of the $\gamma\mathbf{d} \to \pi^0 np$ reaction at photon lab-energy $E_\gamma = 349 \pm 5$ MeV have been measured by the LEGS@BNL Collaboration [14]. However, the data analysis has not yet been completed.

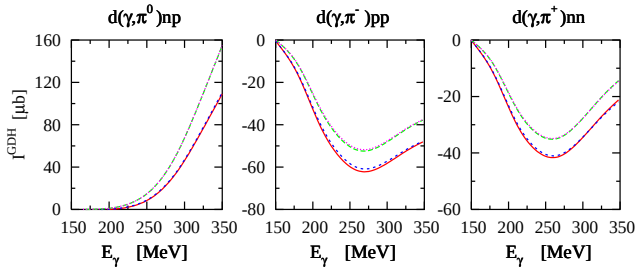

Fig. 21: The Gerasimov-Drell-Hearn integral (see Eq. (46) for its definition) as a function of the upper integration limit for separate channels of the $\mathbf{d}(\gamma,\pi)NN$ reaction. Curve conventions as in Fig. (11).

4.3.6 The Gerasimov-Drell-Hearn integral

Next, we discuss the GDH sum rule [28] which links the anomalous magnetic moment of a particle to the energy weighted integral of the spin asymmetry of the photo-absorption cross section. For a particle of mass M, charge eQ, anomalous magnetic moment κ, and spin S it reads

$$I^{GDH} = \int_0^\infty \frac{dE'_\gamma}{E'_\gamma}\left(\sigma^P(E'_\gamma) - \sigma^A(E'_\gamma)\right) = 4\pi^2\kappa^2\frac{e^2}{M^2}S\,, \tag{46}$$

where $\sigma^{P(A)}$ denote the total absorption cross sections for circularly polarized photons on a target with spin parallel (P) and antiparallel (A) to the photon spin. This sum rule provides a very interesting relation between a ground state property (κ) of a particle and its whole excitation spectrum. Apart from the general assumption that the integral in Eq. (46) converges, its derivation is based solely on first principles like Lorentz and gauge invariances, unitarity, crossing symmetry, and causality of the Compton scattering amplitude of a particle. Consequently, from the experimental and theoretical points of view, a test for various targets becomes very important.

To present the results in a direct way, we introduce the finite GDH integral as defined by

$$I^{GDH}(E_\gamma) = \int_0^{E_\gamma} \frac{dE'_\gamma}{E'_\gamma}\left(\sigma^P(E'_\gamma) - \sigma^A(E'_\gamma)\right)\,. \tag{47}$$

In Fig. (21) we depict our results for the evaluation of the GDH integral for the individual contributions from the different charge states of the pion for the $\gamma d \to \pi NN$ reaction as a function of the upper integration limit. The contributions of various pion photoproduction channels to the finite GDH integral (Eq. (47)) up to 350 MeV and their sum are summarized in Table (1) (see also Ref. [29]).

We find that a large positive contribution to the GDH integral comes from the π^0-production channel, whereas the charged pion channels give a negative but - in absolute value - smaller contribution to the GDH integral. This negative contribution comes from the isovector M1 transition to the $^1S_0$ state, which can only be accessed when the spins of the photon and the deuteron are antiparallel. The inclusion of NN-rescattering reduces significantly (more than a half, see Table (1)) the value of the integral. The integral is slightly reduced by the πN-rescattering. Contrary with what we have found in other observables, we find that FSI effects are sizeable in the GDH integral for both neutral and charged pion production channels [29]. The measurement of spin asymmetry for the various pion photoproduction channels on the deuteron represents a stringent test of our present theoretical understanding of the $\gamma d \to \pi NN$ reaction. Hence, the experimental programs at facilities like MAMI at Mainz and ELSA at Bonn, concerning the GDH sum

Table 1: *Contributions of various channels for quasifree pion photoproduction from the deuteron to the finite GDH integral using the elementary reaction from [31] and explicitly integrated up to a photon lab-energy of 350 MeV in μb.*

Contribution	$\pi^- pp$	$\pi^+ nn$	$\pi^0 np$	πNN
IA	-36.08	-13.07	155.93	106.78
IA+NN	-46.28	-20.37	111.04	44.39
IA+NN+πN	-47.76	-20.11	109.16	41.29

rule on the deuteron are of great importance for further progress in the field.

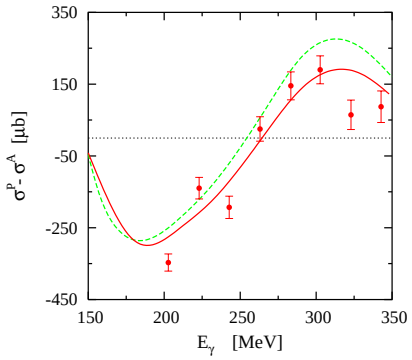

Fig. 22: The helicity-dependent total photoabsorption cross section difference $(\sigma^P - \sigma^A)$ for the semiexclusive channels $\gamma\mathbf{d} \to \pi^{\pm} NN$. Curve conventions: dashed, IA$^* + NN + \pi N_c$ using MAID [26]; solid, IA+$NN + \pi N$ using the bare electromagnetic multipoles of ELA [31]. Experimental data taken from [13].

4.4 Sensitivity to the elementary $\gamma N \to \pi N$ amplitude

In what follows, we discuss the influence of different choices for the input elementary pion photoproduction operator on the results presented above for the $\gamma\mathbf{d} \to \pi NN$ reaction channels (see Refs. [29,30] for more results). We compare results for the helicity total and differential cross sections, spin asymmetries, and the GDH sum rule for the deuteron in the energy region from near π-threshold to the $\Delta(1232)$-resonance, using as elementary reaction amplitudes the ones provided by the ELA model from Ref. [31] and those obtained using MAID model [26]. The results of this comparison are collected in Figs. (22), (23), (24), and (25)).

First, in Fig. (22) we show the helicity-dependent total photoabsorption cross section difference $(\sigma^P - \sigma^A)$ for the semi-exclusive channels $\gamma\mathbf{d} \to \pi^{\pm} NN$ using the elementary operators from MAID (dashed curve) and our

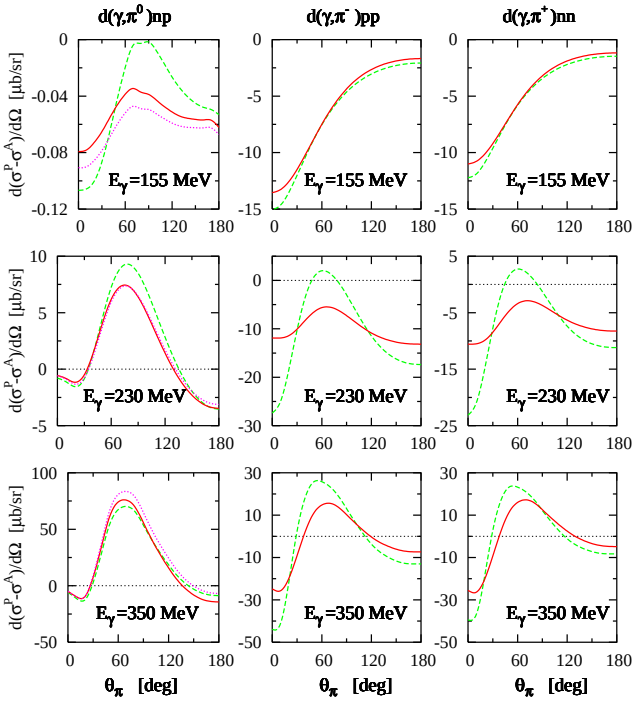

Fig. 23: Circular photon polarization asymmetry for the separate channels of semi-exclusive pion photoproduction on the deuteron as a function of the pion angle in the laboratory frame at various photon lab-energies using different elementary pion photoproduction operators and including FSI effects. Curve conventions: dashed, IA$^* + NN + \pi N_c$ using MAID [26]; dotted, IA$^* + NN + \pi N_c$ using the dressed multipoles of ELA [31]; solid, IA+$NN + \pi N$ using the bare electromagnetic multipoles of ELA.

ELA model (solid curve) including FSI effects. We compare to the latest experimental data from the A2 and GDH@MAMI Collaborations [13] and we find an excellent agreement with data. Our ELA computation provides a slightly better agreement than the computation using MAID model.

In Fig. (23) we show the helicity differential cross section difference $d(\sigma^P - \sigma^A)/d\Omega$ using the bare ELA model (solid), using MAID model (dashed) and the dressed ELA model (dotted) in the neutral channel. Both results are quite different, specially at low energies. At the peak position, we obtain larger values using MAID than using ELA. At extreme forward pion angles, large differences between both results is obtained. This discrepancy is more noticeable for energies close to π-threshold and shows up the differences among elementary operators. The difference between the dotted (dressed ELA) and solid (bare ELA) curves shows the effect of πN-rescattering, which is found to be important near π-threshold.

If we focus our attention on the E-asymmetry (Fig. (24)) and GDH integral (Fig. (25)), a sizeable difference is obtained in the energy region near π-threshold. Table

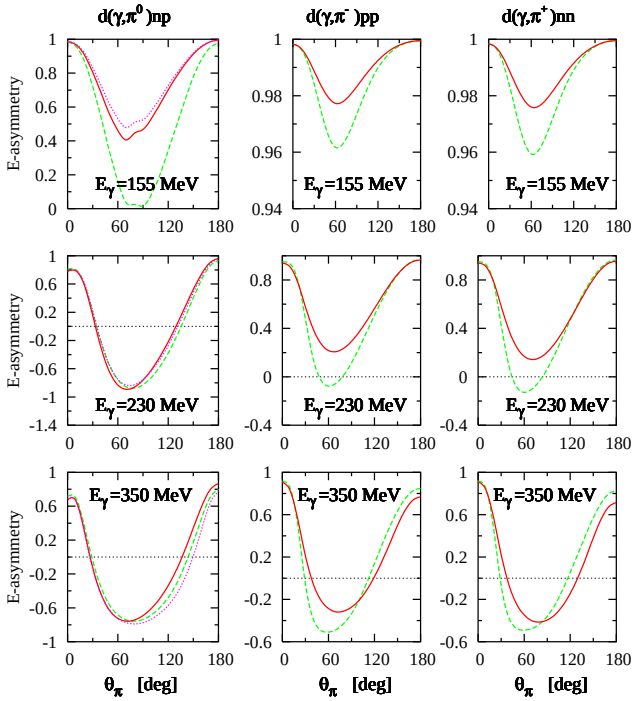

Fig. 24: The double polarization E-asymmetry as a function of the pion angle in the laboratory frame at various photon lab-energies for the separate channels of $\mathbf{d}(\gamma,\pi)NN$ using different elementary pion photoproduction operators and including FSI effects. Curve conventions as in Fig. (23).

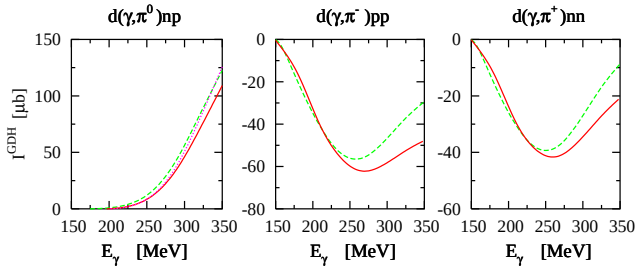

Fig. 25: The Gerasimov-Drell-Hearn integral as a function of the upper integration limit for separate channels of the $\mathbf{d}(\gamma,\pi)NN$ reaction using different elementary pion photoproduction operators and including FSI effects. Curve conventions as in Fig. (23).

(2) displays the extracted values of the GDH integral up to 350 MeV for all three pion photoproduction channels and their sum for our results using MAID as elementary reaction operator. Compared the values in Table (2) using MAID to the values presented in Table (1) using ELA, we find that ELA: $I_{IA}^{GDH}(350\ \text{MeV}) = 106.78\ \mu$b whereas MAID: $I_{IA^*}^{GDH}(350\ \text{MeV}) = 147.47\ \mu$b. After including FSI effects we obtained ELA:

Table 2: *Same as Table (1) but using the MAID model [26] as elementary reaction operator.*

Contribution	$\pi^- pp$	$\pi^+ nn$	$\pi^0 np$	πNN
IA^*	-23.02	-3.87	174.36	147.47
$\text{IA}^* + NN$	-28.79	-8.65	123.13	85.69
$\text{IA}^* + NN + \pi N_c$	-29.38	-8.68	122.67	84.61

$I_{IA+NN+\pi N}^{GDH}(350\ \text{MeV}) = 41.29\ \mu$b whereas MAID: $I_{IA^*+NN+\pi N_c}^{GDH}(350\ \text{MeV}) = 84.61\ \mu$b (see also Ref. [29]).

In the charged channels the results using MAID or ELA as elementary reaction operators are different in the near π-threshold region, where the predicted E-asymmetry within the ELA is - in negative sign - smaller than those within MAID, but provide similar results in the $\Delta(1232)$-region. Although both computations provide results for the GDH integral that differ in, approximately, a factor two, the curves computed using MAID and ELA models displayed in Fig. (22) are not much different, and one must look more in deep for the reasons in the different GDH values. This large difference in the GDH - in spite of the relatively small dissimilarity shown in Fig. (22) - shows the large sensitivity of the GDH integral to the choice of the elementary operator employed. The GDH results from two large contributions of negative and positive signs, that cancel to a large extent in the final results. The curve computed with the MAID model seems more "symmetric" and hence the cancellation of the positive and the negative contributions to the integral is larger than for the ELA model computation which presents a larger – in absolute value – negative part. This partial cancellation also means that the contribution of the processes considered in this work to the total GDH integral up to 350 MeV is relatively small compared to other contributions. For instance in Ref. [24] a value of about 240 μb for the total GDH integral up to 350 MeV is found. Our pionic contributions gives 42 μb. The rest should be either coherent pion production or two-nucleon break-up. Summarizing, we can say that the MAID model provides different predictions for polarization observables than the ELA model, particularly at low photon energies, and that the GDH integral provides an excellent observable to test different pion production operators.

From the preceding discussion it is apparent that πN-rescattering and the choice of the elementary operator have a visible effect on spin observables. Therefore, we have to be careful when including additional πN-rescattering in calculations that use MAID or SAID as elementary reaction operator.

5 Conclusions and outlook

The main topic of this work was the investigation of polarization observables in incoherent pion

photoproduction from the deuteron in the energy region from π-threshold up to the $\Delta(1232)$-resonance with inclusion of all *leading* πNN effects. Formal expressions for polarization observables are derived and described by various beam, target and beam-target asymmetries for polarized photons and/or polarized deuterons. For the elementary pion photoproduction operator on the free nucleon, a realistic effective Lagrangian approach is used which includes seven nucleon resonances, in addition to Born and vector-meson exchange terms. The interactions in the final two-body subsystems are taken from separable representations of realistic potentials. Results are given for the unpolarized cross sections, the doubly polarized cross sections for parallel and antiparallel helicity states, the linear photon asymmetry, the double polarization E-asymmetry, the vector and tensor deuteron asymmetries for the $\gamma\mathbf{d} \to \pi^- pp$, $\gamma\mathbf{d} \to \pi^+ nn$, and $\gamma\mathbf{d} \to \pi^0 np$ channels. Contributions from various channels to the spin asymmetry and the GDH integral are evaluated by explicit integration up to a photon lab-energy of 350 MeV. The sensitivity to the elementary $\gamma N \to \pi N$ operator of the results has also been investigated.

Within our model, we have found that the inclusion of FSI effects is important for unpolarized cross sections. It leads to a reduction (an overestimation) of the total cross section for π^0 ($\pi^\pm$) production. πN-rescattering appears to be less important compared to the NN-rescattering in both neutral and charged channels. Compared to experimental data, we have found that the sizeable discrepancies without rescattering are largely reduced and that a quite good agreement with the data is achieved. With respect to the ChPT prediction from Ref. [49] for the total cross section of π^+ production near π-threshold, we have obtained good agreement when FSI is included.

For the polarized total cross sections σ^P and σ^A as well as spin asymmetry $\sigma^P - \sigma^A$, we have found that the influence of FSI stems predominantly from NN-rescattering, whereas πN-rescattering is much smaller and appears only in σ^A close to π-threshold. In the neutral channel, we have observed that FSI effects lead to a strong reduction of the spin asymmetry and that σ^P is larger than σ^A. In charged channels, we have found that FSI effects appear mainly in σ^A near π-threshold. We have also found that $\sigma^P - \sigma^A$ starts out negative due to the E_{0+} multipole, and has a strong positive contribution at higher energies due to the M_{1+} multipole.

The results of spin asymmetries are found to be very sensitive to the FSI effects, in particular in the case of the π^0 production channel. We have compared our results to the presently available experimental data. A qualitative and quantitative agreement with the data of Σ-asymmetry from LEGS [14] are obtained after including the FSI effects. With respect to the prediction without FSI of Lee-Sato [51] for the Σ-asymmetry of π^--production channel, good agreement is found too. Regarding the results of the E-asymmetry, qualitatively a similar behavior for all channels is found. We have also found that the influence of the FSI effects is strong, especially in the neutral channel at forward angles and low energies. The contributions of separate channels to the GDH integral are evaluated by explicit integration up to 350 MeV. A total value of the GDH integral of $I^{GDH}_{IA+NN+\pi N}(350\ \text{MeV}) = 41.29\ \mu$b has been computed after including FSI effects. A large positive contribution to the GDH integral came from the π^0-production channel whereas the charged pion channels gave a negative but – in absolute value – smaller contribution to the GDH integral.

We have also studied the influence of the elementary operator on the unpolarized cross sections, polarized cross sections, spin asymmetries, and GDH integral. All observables, specially the spin asymmetries for both the neutral and charged channels, are found to be very sensitive to the elementary operator. In many cases the deviation among results obtained using different operators is very large. It is shown also that the process $d(\gamma,\pi)NN$ can serve as a filter for different elementary operators since its cross section and asymmetry predictions show very different values when one varies the elementary pion production operators employed.

The GDH integral is found to be an excellent observable to discriminate among different elementary pion production operators. We obtain quite different values for the GDH integral for the MAID and the ELA models, in spite of the fact that their predictions for the $\sigma^P - \sigma^A$ observable seem similar (see Fig. (22)). Due to an important cancelation of the contributions below and above a photon energy of 260 MeV the pionic contribution to the GDH integral up to 350 MeV computed in this work gives 42 μb, what is relatively small compared to other contributions. The rest should be either coherent pion production or two-nucleon break-up [24].

Finally, we would like to point out that future improvements of the present model (in particular, its extension to higher energies) can be achieved by including the next leading correction from the intermediate NN, NN^*, and $N\Delta$ interactions. Polarization observables in general constitute more stringent tests for theoretical models due to their sensitivity to small amplitudes. At this point, a much needed measurement on the deuteron spin asymmetries will certainly provide us with an important observable to test our knowledge of the pion photoproduction on the neutron process and, hence, to provide us with valuable information on the neutron spin asymmetry in an indirect way. An independent test within the framework of effective field theory will be also of great interest. Moreover, the formalism can also be extended to investigate polarization observables of pion electroproduction on the deuteron where the virtual photon has more degrees of freedom than the real one. Therefore, it can be used to explore the reaction more deeply.

Acknowledgements

I am gratefully acknowledge very useful discussions with T.-S.H. Lee, T. Sato, H. Arenhövel, C. Fernández-Ramírez, E. Moya de Guerra, and J.M. Udías. I am deeply indebted to the members of the GDH and A2 Collaborations, especially J. Ahrens and P. Pedroni, the TAPS Collaboration, specially B. Krusche, and the LEGS Collaboration, specially A.M. Sandorfi and M. Lucas, for providing me with their experimental data.

References

[1] G. F. Chew and H. W. Lewis, Phys. Rev. **84**, 779 (1951).
[2] M. Lax and H. Feshbach, Phys. Rev. **88**, 509 (1952).
[3] I. Blomqvist and J. M. Laget, Nucl. Phys. A **280**, 405 (1977).
[4] J. M. Laget, Nucl. Phys. A **296**, 388 (1978).
[5] J. M. Laget, Phys. Rep. **69**, 1 (1981).
[6] R. Schmidt, H. Arenhövel, and P. Wilhelm, Z. Phys. **A355**, 421 (1996).
[7] M.I. Levchuk, M. Schumacher, and F. Wissmann, arXiv:nucl-th/0011041.
[8] E.M. Darwish, H. Arenhövel, and M. Schwamb, Eur. Phys. J. A **16**, 111 (2003).
[9] E.M. Darwish, H. Arenhövel, and M. Schwamb, Eur. Phys. J. A **17**, 513 (2003).
[10] I. T. Obukhovsky *et al.*, J. Phys. G: Nucl. Part. Phys. G **29**, 2207 (2003).
[11] B. Krusche *et al.*, Eur. Phys. J. A **6**, 309 (1999); B. Krusche and S. Schadmand, Prog. Part. Nucl. Phys. **51**, 399 (2003); V. Burkert and T.-S.H. Lee, Int. J. Mod. Phys. E **13**, 1035 (2004); D. Drechsel and L. Tiator, Ann. Rev. Nucl. Part. Sci. **54**, 69 (2004); H. Dutz *et al.*, Phys. Rev. Lett. **93**, 032003 (2004); K. Helbing, Prog. Part. Nucl. Phys. **57**, 405 (2006).
[12] P. Pedroni, private communication; C.A. Rovelli, Diploma thesis, University of Pavia, Italy (2002); O. Jahn, in Proceedings of the 3rd International Symposium on the Gerasimov-Drell-Hearn Sum Rule and its Extensions (GDH 2004), Norfolk, Virginia, June 1-5 (2004); A. Braghieri, in Proceedings of the 10th International Conference on the Structure of Baryons (BARYONS 2004), Ecole Polytechnique, Polaiseau, France, Oct. 25-29 (2004); A. Thomas and M. Martínez, in Proceedings of the Symposium of Twenty Years of Physics at the Mainz Microtron (MAMI), J. Gutenberg-Universität, Mainz, Germany, Oct. 19-22 (2005); T. Rostomyan, PhD dissertation, Gent University (2005); H.-J. Arends, in Proceedings of the 9th Conference on the Intersections of Particle and Nuclear Physics (CIPNP 2006), Westin Rio Mar Beach, Puerto Rico, May 30-June 03 (2006); T. Rostomyan and P. Pedroni, in 23rd Students' Workshop on Electromagnetic Interactions, Bosen (Saar), Germany, Sept. 3-8 (2006); A. Thomas, Eur. Phys. J. A **28**, Suppl. 1, 161 (2006); M. Martínez, PhD dissertation, J. Gutenberg-Universität, Mainz, Germany.
[13] J. Ahrens *et al.*, Phys. Rev. Lett. **97**, 202303 (2006); Phys. Rev. Lett. **98**, 039901(E) (2007).
[14] LEGS@BNL Collaboration, A.M. Sandorfi and M. Lucas, private communication; M. Lucas, in *LOWq 2001 Workshop on Electromagnetic Nuclear Reactions at Low Momentum Transfer*, Halifax, Nova Scotia, Canada, 23-25 August, 2001.
[15] A. Loginov, A. Sidorov, and V. Stibunov, Phys. Atom. Nucl. **63**, 391 (2000) [Yad. Fiz. **63**, 459 (2000)].
[16] E. M. Darwish, Nucl. Phys. A **735**, 200 (2004).
[17] E.M. Darwish, Int. J. Mod. Phys. E **13**, 1191 (2004).
[18] E.M. Darwish, J. Phys. G **31**, 105 (2005).
[19] E.M. Darwish, Prog. Theor. Phys. **113**, 169 (2005).
[20] E.M. Darwish, Phys. Lett. B **615**, 61 (2005).
[21] E.M. Darwish and A. Salam, Nucl. Phys. A **759**, 170 (2005).
[22] E.M. Darwish and M. El-Zohry, Phys. Scr. **75**, 738 (2007).
[23] H. Arenhövel and A. Fix, Phys. Rev. C **72**, 064004 (2005); A. Fix and H. Arenhövel, Phys. Rev. C **72**, 064005 (2005).
[24] H. Arenhövel, A. Fix, and M. Schwamb, Phys. Rev. Lett. **93**, 202301 (2004); H. Arenhövel, A. Fix, and M. Schwamb, in Proceedings of the 3rd International Symposium on the Gerasimov-Drell-Hearn Sum Rule and its Extensions (GDH 2004), Norfolk, Virginia, June 1-5, (2004), arXiv:nucl-th/0409015.
[25] M.I. Levchuk, A.Yu. Loginov, A.A. Sidorov, V.N. Stibunov, and M. Schumacher, Phys. Rev. C **74**, 014004 (2006).
[26] D. Drechsel, O. Hanstein, S. Kamalov, and L. Tiator, Nucl. Phys. A **645**, 145 (1999); MAID Program, http://www.kph.uni-mainz.de/MAID/maid2003/.
[27] R.A. Arndt, W.J. Briscoe, I.I. Strakovsky, and R.L. Workman, Phys. Rev. C **66**, 055213 (2002), SAID database, http://gwdac.phys.gwu.edu.
[28] S.B. Gerasimov, Sov. J. Nucl. Phys. **2**, 430 (1966) [Yad. Fiz. **2**, 598 (1965)]; S.D. Drell and A.C. Hearn, Phys. Rev. Lett. **16**, 908 (1966).
[29] E.M. Darwish, C. Fernández-Ramírez, E. Moya de Guerra, and J.M. Udías, Phys. Rev. C **76**, 044005 (2007).
[30] E.M. Darwish and S. Al-Thoyaib, Ann. Phys. **326**, 604 (2011).
[31] C. Fernández-Ramírez, E. Moya de Guerra, and J.M. Udías, Ann. Phys. (N.Y.) **321**, 1408 (2006); C. Fernández-Ramírez, PhD dissertation, Universidad Complutense de Madrid, Spain (2006).
[32] J.D. Bjorken and S.D. Drell, *Relativistic Quantum Mechanics* (McGraw-Hill, New York, 1964).
[33] J. Lippmann and W. Schwinger, Phys. Rev. **84**, 1232 (1951).
[34] Review of Particle Physics, W.-M. Yao *et al.*, J. Phys. G **33**, 1 (2006).
[35] D.G. Ireland, S. Janssen, and J. Ryckebusch, Nucl. Phys. A **740**, 147 (2004).
[36] E.M. Darwish, PhD dissertation, J. Gutenberg-Universität, Mainz, Germany (2002).
[37] J. Haidenbauer and W. Plessas, Phys. Rev. C **30**, 1822 (1984); J. Haidenbauer and W. Plessas, Phys. Rev. C **32**, 1424 (1985).
[38] S. Nozawa, B. Blankleider, and T.-S.H. Lee, Nucl. Phys. A **513**, 459 (1990).
[39] M. Lacombe *et al.*, Phys. Rev. C **21**, 861 (1980); M. Lacombe *et al.*,Phys. Lett. **B101**, 139 (1981).
[40] H. Arenhövel, Few-Body Syst. **4**, 55 (1988).
[41] B. A. Robson, *The Theory of Polarization Phenomena* (Clarendon Press, Oxford, 1974).
[42] A. R. Edmonds, *Angular Momentum in Quantum Mechanics* (Princeton University Press, New Jersey, 1957).
[43] J. Ahrens *et al.*, Eur. Phys. J. A **21**, 323 (2004); I. Preobrajenski, Dissertation, Institut für Kernphysik, Johannes Gutenberg-Universität, Mainz, (2001).

[44] H. Garcilazo and T. Mizutani, *πNN Systems*, (World Scientific, Singapore, 1990).
[45] P. Benz *et al.*, Nucl. Phys. B **65**, 158 (1973).
[46] G. Chiefari, E. Drago, M. Napolitano, and C. Sciacca, Lett. Nuovo Cim. **13**, 129 (1975).
[47] M.A. Quraan *et al.*, Phys. Rev. C **57**, 2118 (1998).
[48] E.C. Booth, B. Chasan, J. Comuzzi, and P. Bosted, Phys. Rev. C **20**, 1217 (1979).
[49] V. Lensky, V. Baru, J. Haidenbauer, C. Hanhart, A. Kudryavtsev, and U.-G. Meißner, Eur. Phys. J. A **26**, 107 (2005).
[50] I. Duck, Phys. Lett. B **59**, 9 (1975); J.V. Noble, Phys. Lett. B **67**, 39 (1977).
[51] T.-S.H. Lee and T. Sato, private communication.
[52] T. Sato and T.-S.H. Lee, Phys. Rev. C **54**, 2660 (1996); T. Sato and T.-S.H. Lee, Phys. Rev. C **63**, 055201 (2001).

Eed M. Darwish is an Associate Professor of Physics at Sohag University, Egypt. He received his PhD degree in Theoretical Nuclear Physics from the Johannes-Gutenberg University, Mainz, Germany as a DAAD scholarship. Then he became a Faculty Member at Sohag University for six years. He became Assistant Professor of Physics at Sohag University in 2002 and Associate Professor in 2013. He joined Taibah University, Saudi Arabia as an Associate Professor (on leave) in 2008. He has served as Head of Applied Physics Department at Taibah University in 2009-2011. His research includes work on the study of sub-nuclear degrees of freedom in electromagnetic reactions in few-body systems, mainly the deuteron, e.g. photo- and electro-production of pseudo-scalar mesons on the deuteron including polarization observables. He has published more than 60 research papers in reputed international journals of physics. He is referee of several international physics journals.